



Contents lists available at ScienceDirect

## Progress in Oceanography

journal homepage: [www.elsevier.com/locate/pocean](http://www.elsevier.com/locate/pocean)

## A tale of two gyres: Contrasting distributions of dissolved cobalt and iron in the Atlantic Ocean during an Atlantic Meridional Transect (AMT-19)

Rachel U. Shelley<sup>a,\*,1</sup>, Neil J. Wyatt<sup>a,2</sup>, Glenn A. Tarran<sup>b</sup>, Andrew P. Rees<sup>b</sup>, Paul J. Worsfold<sup>a</sup>, Maeve C. Lohan<sup>a,3</sup>

<sup>a</sup> Plymouth University, School of Geography, Earth and Environmental Sciences, Drake Circus, Plymouth PL4 8AA, UK

<sup>b</sup> Plymouth Marine Laboratory, Prospect Place, Plymouth PL1 3DH, UK

## ARTICLE INFO

## Article history:

Available online xxx

## ABSTRACT

Cobalt (Co) and iron (Fe) are essential for phytoplankton nutrition, and as such constitute a vital link in the marine biological carbon pump. Atmospheric deposition is an important, and in some places the dominant, source of trace elements (TEs) to the global ocean. Dissolved cobalt (dCo) and iron (dFe) were determined along an Atlantic Meridional Transect (AMT-19; Oct/Nov 2009) between 50°N and 40°S in the upper 150 m in order to investigate the behaviour and distribution of these two essential, bioactive TEs. During AMT-19, large differences in the distributions of dCo and dFe were observed. In the North Atlantic gyre provinces, extremely low mixed layer dCo concentrations ( $23 \pm 9$  pM) were observed, which contrasts with the relatively high mixed layer dFe concentrations (up to 1.0 nM) coincident with the band of highest atmospheric deposition ( $\sim 5$ – $30^\circ$ N). In the South Atlantic gyre, the opposite trend was observed, with relatively high dCo ( $55 \pm 18$  pM) observed throughout the water column, but low dFe concentrations ( $0.29 \pm 0.08$  nM). Given that annual dust supply is an order of magnitude greater in the North than the South Atlantic, the dCo distribution was somewhat unexpected. However, the distribution of dCo shows similarities with the distribution of phosphate ( $\text{PO}_4^{3-}$ ) in the euphotic zone of the Atlantic Ocean, where the North Atlantic gyre is characterised by chronically low  $\text{PO}_4$ , and higher concentrations are observed in the South Atlantic gyre (Mather et al., 2008), suggesting the potential for a similar biological control of dCo distributions. Inverse correlations between dCo and *Prochlorococcus* abundance in the North Atlantic gyre provinces, combined with extremely low dCo where nitrogen fixation rates were highest ( $\sim 20$ – $28^\circ$ N), suggests the dominance of biological controls on dCo distributions. The contrasting dCo and dFe distributions in the North and South Atlantic gyres provides insights into the differences between the dominant controls on the distribution of these two bioactive trace metals in the central Atlantic Ocean.

© 2016 Elsevier Ltd. All rights reserved.

### 1. Introduction

Cobalt (Co), like iron (Fe), is essential for phytoplankton growth (e.g. Morel et al., 1994; Saito et al., 2002; Sunda and Huntsman, 1995a, 1995b; Timmermans et al., 2001; Rodriguez and Ho, 2015). Cobalt is the metal centre in the vitamin B<sub>12</sub> (cobalamin) complex which is essential for the synthesis of amino acids,

deoxyriboses, and the reduction and transfer of single carbon fragments in many biochemical pathways. Cobalt is required for the de novo synthesis of vitamin B<sub>12</sub> by marine prokaryotes (Bonnet et al., 2010). However, the majority of eukaryotic marine phytoplankton are B vitamin auxotrophs, acquiring their vitamin B<sub>12</sub> requirements through a symbiotic relationship with bacteria (Croft et al., 2005; Cruz-López and Maske, 2016), although this pathway might not be a simple linear flux from producer to consumer (Helliwell et al., 2016). Cobalt is also the metal co-factor in the metalloenzyme, carbonic anhydrase (CA), which is required for inorganic carbon acquisition by *Prochlorococcus*, and *Synechococcus* (Sunda and Huntsman, 1995a; Saito et al., 2002). In addition, *Trichodesmium* require Co for nitrogen fixation (Rodriguez and Ho, 2015), and Co can substitute for zinc (Zn) as the metal co-factor of the protein PhoA in the enzyme alkaline phosphatase (AP) (Gong et al., 2005; Sunda and Huntsman, 1995a). The production of AP facilitates

\* Corresponding author.

E-mail address: [rachel.shelley@univ-brest.fr](mailto:rachel.shelley@univ-brest.fr) (R.U. Shelley).

<sup>1</sup> Laboratoire des Sciences de l'Environnement Marin, UMR 6539 LEMAR (CNRS/UBO/IRD/IFREMER), Institut Universitaire Européen de la Mer, Technopôle Brest-Iroise, Plouzané, 29280, France.

<sup>2</sup> School of Earth, Ocean and Atmospheric Science, Florida State University, 117 N. Woodward Ave., Tallahassee, FL 32306, USA.

<sup>3</sup> University of Southampton Waterfront Campus, National Oceanography Centre, European Way, Southampton, SO14 3ZH, UK.

<http://dx.doi.org/10.1016/j.pocean.2016.10.013>

0079-6611/© 2016 Elsevier Ltd. All rights reserved.

acquisition of phosphorus (P) from the organic-P pool by phytoplankton and bacteria (e.g. Mahaffey et al., 2014). In addition, the strong correlation between dissolved Co (dCo) and inorganic-P (phosphate, PO<sub>4</sub>) in the upper water column, across diverse oceanic regimes (Saito and Moffett, 2002; Noble et al., 2008, 2012; Bown et al., 2011; Dulaquais et al., 2014a; Baars and Croot, 2015), indicates the nutritive role of Co.

The role of iron (Fe) as an essential requirement for phytoplankton growth is well documented (e.g. Martin, 1990; Coale et al., 1996; Boyd et al., 2007). For example, photosystems I and II are Fe intensive, and Fe is required for enzymatic process at nearly all stages of the microbial nitrogen cycle, including nitrogen fixation (Morel and Price, 2003; Küpper et al., 2008; Richier et al., 2012). Despite Fe being the fourth most abundant element in the Earth's crust, dissolved Fe (dFe) is often only present at trace concentrations (<0.5 nM) in oxygenated surface waters of the open ocean (Blain et al., 2007; Measures et al., 2008; Ussher et al., 2013). Consequently, primary production is limited by low Fe-availability in 30–40% of the world's oceans (Moore et al., 2002; Boyd and Ellwood, 2010). In the Atlantic Ocean, a number of studies have demonstrated that primary production can be under Fe-stress or limitation, seasonally in association with the spring bloom. (Moore et al., 2006; Nielsdottir et al., 2009), as well as in regions where subsurface nutrient supply is enhanced (Moore et al., 2013, and references therein). The supply of Aeolian Fe is also a key control on the distribution of diazotrophs (Mills et al., 2004; Moore et al., 2009). In addition to Fe, light, macronutrients (N, P, Si), vitamins (e.g. B<sub>12</sub>) and micronutrients (e.g. Co, Zn) may also (co-)limit marine productivity (Bertrand et al., 2007; Saito et al., 2008; Moore et al., 2013; Browning et al., 2014).

A major vector of trace elements (TEs) to Atlantic surface waters is atmospheric deposition (Jickells et al., 2005; Baker et al., 2006, 2007; Sarthou et al., 2007; Buck et al., 2010; Evangelista et al., 2010; Ussher et al., 2013; Shelley et al., 2015), much of which originates from Northwest Africa (Prospero and Carlton, 1972). An estimated 240 ± 80 Tg of dust is transported westwards annually (Kaufman et al., 2005), primarily during the summer months. Approximately 40% of annual global dust deposition occurs in the North Atlantic Ocean (Jickells et al., 2005); the majority of this into waters beneath the Saharan dust plume (~5–30°N) (Mahowald et al., 1999; Prospero et al., 2002; Kaufman et al., 2005). Hence, it is between these latitudes that surface Fe concentrations are highest (Measures et al., 2008; Fitzsimmons et al., 2013; Ussher et al., 2013). Wet deposition in the Intertropical Convergence Zone (ITCZ) scavenges aerosols from the atmosphere, effectively preventing the southwards transport of North African aerosols (Schlosser et al., 2013). Thus the seasonal migration of the ITCZ drives the latitudinal gradient in aerosol dust loading (Prospero and Carlson, 1972; Doherty et al., 2012, 2014; Tsamalis et al., 2013), and hence surface water Fe concentrations and results in a concomitant shift in the latitudinal distribution of diazotrophy and corresponding dissolved inorganic-P depletion (Schlosser et al., 2013). Despite Co being less abundant in crustal material than Fe (Fe 3.9%, Co 0.002%; Rudnick and Gao, 2003), atmospheric deposition is a source of Co to surface waters. (Shelley et al., 2012; Dulaquais et al., 2014a). Consequently, we anticipated that Co concentrations would also be highest under the Saharan plume due to the sheer volume of dust that is deposited.

Another important source of trace metals to remote Atlantic surface waters is through vertical mixing. This mechanism reportedly provides ~5–35% of the dFe input flux to the Atlantic mixed layer (Ussher et al., 2013). Vertical mixing is particularly important in the tropics where elevated sub-surface dFe concentrations are associated with low oxygen, upwelled water (Bergquist and Boyle, 2006; Measures et al., 2008; Fitzsimmons et al., 2013; Ussher et al., 2013). On the other hand, lateral advection of Fe from

shelf regions to the remote Atlantic Ocean is reported to range from minimal (Laes et al., 2007; Ussher et al., 2007; Noble et al., 2012; Fitzsimmons et al., 2013) to significant in the vicinity of 20°N (Rijkenberg et al., 2012). For Co, understanding the contribution of these sources is hindered by a relative paucity of data. However, lateral transport has recently been reported in both the eastern and western basins of the Atlantic (Noble et al., 2012; Dulaquais et al., 2014a, 2014b).

Iron and Co distributions are also strongly influenced by both redox speciation and organic complexation. Although Fe<sup>2+</sup> is the more bioavailable form of Fe (Shaked and Lis, 2012), the thermodynamically favoured species of Fe in oxic seawater (pH 8) is Fe<sup>3+</sup>. However, Fe<sup>3+</sup> is relatively insoluble under these conditions, and is rapidly scavenged from the water column and forms insoluble Fe<sup>3+</sup> oxyhydroxides (Liu and Millero, 2002). Chelation by organic ligands increases the solubility of Fe in seawater; both strong (e.g. siderophores) and weaker ligand classes (e.g., humics) have been shown to play a role in maintaining Fe in solution (Mawji et al., 2008; Croot and Heller, 2012; Heller et al., 2013; Buck et al., 2015). Similarly, Co<sup>2+</sup> is also thermodynamically favoured in oxic seawater, and Co forms strong organic complexes (Ellwood and van den Berg, 2001; Saito and Moffett, 2001; Baars and Croot, 2015).

The primary removal mechanism for Co and Fe from the euphotic zone is through biological uptake (Martin and Gordon, 1988; Moffett and Ho, 1996). In addition, adsorptive scavenging on to particles (Moffett and Ho, 1996; Johnson et al., 1997; Wu et al., 2001; Bruland and Lohan, 2003) and aggregation and sinking (Croot et al., 2004) are also important removal pathways for both Co and Fe.

The Atlantic Meridional Transect (AMT) programme provides an ideal platform to investigate Co and Fe cycling in the upper Atlantic Ocean and the role of these metals on climate-relevant biological processes. Here we report the geographical distribution and biogeochemistry of Co and Fe in the upper water column along a 12,000 km, gyre-centred transect of the Atlantic Ocean (AMT-19) between ~50°N and 40°S. As our knowledge of Fe biogeochemistry is arguably more advanced than for Co, the following discussion aims to develop our understanding of Co biogeochemistry in the upper water column (≤150 m) of the Atlantic Ocean between 50°N and 40°S by making comparisons with dissolved Fe distributions from this and earlier studies.

## 2. Materials and methods

### 2.1. Sampling

Twenty-nine stations were sampled during cruise AMT-19 (13/10/09–28/11/09) from Falmouth, UK to Punta Arenas, Chile, on board the R.R.S. *James Cook* (Fig. 1). Stations were sampled from the six biogeographical provinces listed in Fig. 1, described by Longhurst (1998). In this study, the distribution of salinity, temperature, dCo, dFe and macronutrients (nitrate and phosphate) were used to identify the province boundaries (Table 1). The assigned province boundaries are subject to small-scale variations due to their seasonal drift, as is the ITCZ, a region that forms the boundary between the atmospheric hemispheres which migrates seasonally from a position centred at ~5°N in boreal winter to ~10°N in the boreal summer (Sultan and Janicot, 2000).

Samples for the determination of dCo and dFe were collected from 10 L trace metal-clean Teflon coated Ocean Test Equipment (OTE) bottles, attached to a titanium CTD rosette. Samples for macronutrients were collected from ten depths during each titanium CTD rosette deployment to correspond with trace metal sampling, and additionally from standard 20 L Niskin bottles fitted to a

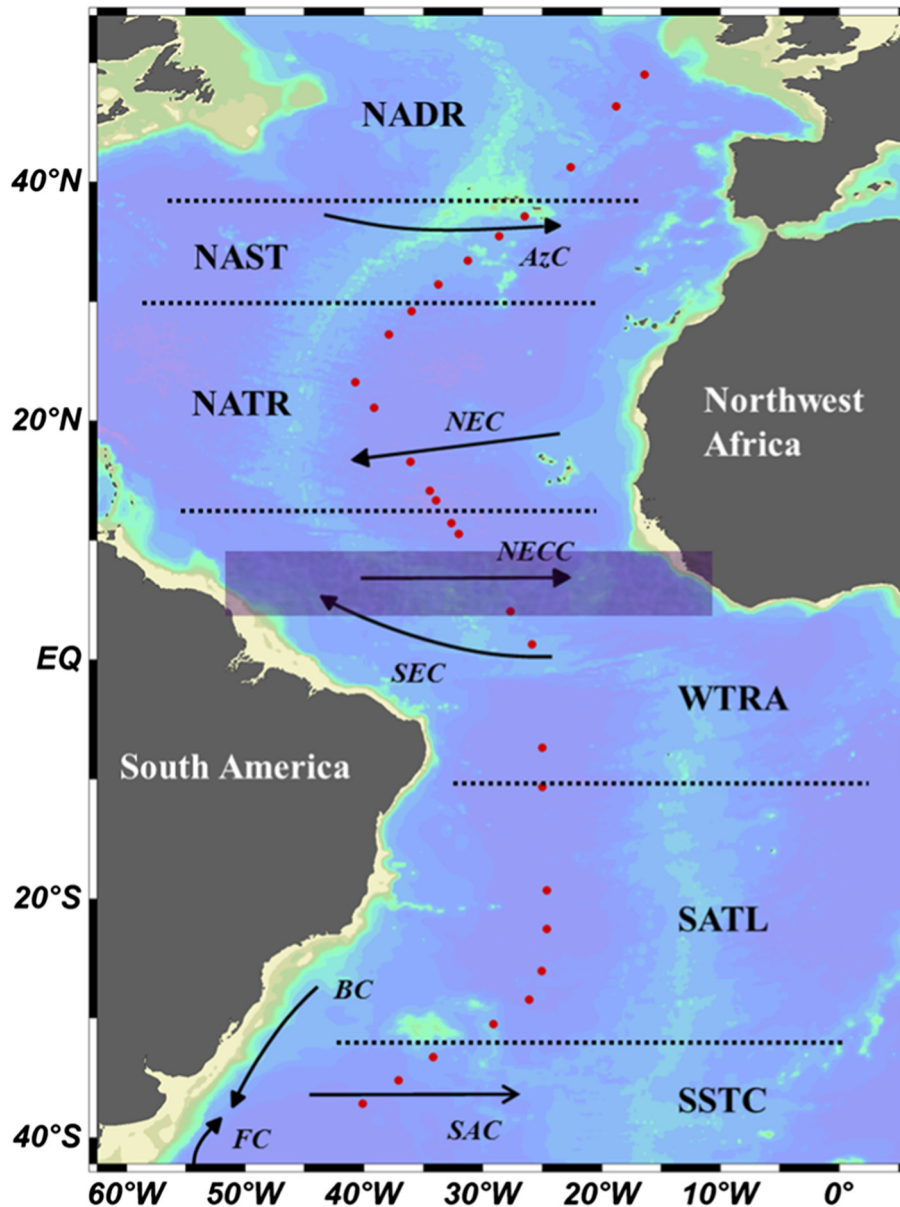


**Fig. 1.** AMT-19 cruise track, showing the 29 water column stations and the biogeochemical provinces (Longhurst, 1998) defined in this study: North Atlantic Drift (NADR, 38–56°N), North Atlantic Gyre (NAST, 30–38°N), North Atlantic Tropical Gyre (NATR, 12–30°N), South Atlantic Gyre (SATL, 10–33°S), and South Atlantic Subtropical Convergence (SSTC, 33–55°S), and Atlantic Ocean surface currents: AzC = Azores Current, NEC = North Equatorial Current, NECC = North Atlantic Counter Current, SEC = South Equatorial Current, BC = Brazil Current, SAC = South Atlantic Current, FC = Falklands Current. The approximate position of the ITCZ (4–9°N with the most intense rain activity between 4 and 5°N) during November 2009 was identified from the Giovanni data product (<http://giovanni.sci.gsfc.nasa.gov>), and is marked by the shaded box.

**Table 1**

Estimation of the contribution of atmospheric dry deposition to the mixed layer (ML) inventories of dCo and dFe. The values used are from: a = Shelley et al. (2015); b = Dulaquais et al. (2014a); c = this study; d = Chance et al. (2015), respectively.

Metal	Location	Dry depo. flux $\mu\text{g m}^{-2} \text{d}^{-1}$	Solubility %	Soluble flux		MLD m	MLD [dCo, dFe] nM		Annual accumulation in ML nM
				$\mu\text{g m}^{-2} \text{d}^{-1}$	$\text{nM m}^{-2} \text{d}^{-1}$		nM	nM	
Cobalt	20 N	1.6 (a)	9.0 (b)	0.14 (a, b)	24 (a, b)	40 (c)	16.2 (c)	0.22	
Cobalt	~20 S	0.0029 (d)	2.0 (d)	0.000058 (d)	0.010 (d)	45 (b)	37 (b)	0.000080	
Iron	20 N	3600 (a)	0.31 (a)	11.2 (a)	201 (a)	40 (c)	0.90 (c)	1.80	
Iron	~20 S	3.2 (d)	2.9 (d)	0.093 (d)	1.7 (d)	45 (c)	0.33 (c)	0.014	

stainless steel CTD rosette (Seabird), thus providing high resolution profiling along the cruise track. All ship-based trace metal sample handling was conducted in a pressurised clean van. Seawater samples for dCo and dFe were filtered into acid-cleaned, low density

polyethylene (LDPE) bottles (Nalgene) using a 0.2  $\mu\text{m}$  Sartobran 300 filter capsule (Sartorius) and acidified to pH 1.7–1.8 (0.024 M) with ultraclean hydrochloric acid (HCl, Romil SpA) inside a class-100 laminar flow hood. Samples for the determination of



TdFe were not filtered prior to acidification to 0.024 M HCl. All samples were then double zip-lock bagged for storage prior to analysis in the home laboratory.

## 2.2. Dissolved cobalt determination

Dissolved Co was determined in the ISO accredited clean room facility (ISO 9001) at Plymouth University, UK by flow injection with chemiluminescence detection (FI-CL; Shelley et al., 2010). Briefly, the flow injection manifold was coupled with a photomultiplier tube (Hamamatsu, model H 6240-01). The dCo was determined in UV-irradiated samples (3 h; 400 W medium-pressure Hg lamp, Photochemical Reactors) from the chemiluminescence produced from the catalytic oxidation of pyrogallol (1,2,3-trihydroxybenzene), the chemiluminescence emission was recorded using LabVIEW v.7.1 software. Due to the extremely stable nature of organic complexes of Co in seawater, several studies have demonstrated the requirement to UV irradiate samples prior to analysis in order to liberate strongly-complexed Co (Vega and van den Berg, 1997; Donat and Bruland, 1988; Saito et al., 2005; Shelley et al., 2010). During all analytical runs UV-irradiated SAFe D2 reference samples were analysed ( $n = 4$ ; measured value,  $50 \pm 2$  pM; consensus value  $46 \pm 3$  pM). Typically, blank values were  $4 \pm 1$  pM ( $n = 8$ ), with a detection limit of 3 pM (blank +  $3\sigma$ ).

## 2.3. Dissolved and total dissolvable iron determination

Dissolved Fe and total dissolvable Fe (TdFe; unfiltered seawater) were also determined using FI-CL in the same clean room facility as the dCo. The Fe FI-CL method used in this study was based on the method originally described by Obata et al. (1993) and modified by de Baar et al. (2008). Briefly, measurements were made based on the catalytic oxidation of luminol (5-amino-2,3-dihydrophthalazine-1,4-dione; Aldrich) by hydrogen peroxide ( $\text{H}_2\text{O}_2$ ) in the presence of Fe. As this method detects Fe(III), this study used a  $\text{H}_2\text{O}_2$  oxidation step whereby  $\text{H}_2\text{O}_2$  (10 nM) was added to each sample 1 h prior to the determination of Fe(III) (Lohan et al., 2005). Chemiluminescence emission was detected by a Hamamatsu photomultiplier tube (model H 6240-01) and recorded using LabVIEW v.7.1 software. The accuracy of the method was assessed for every analytical run by the determination of dFe in SAFe S and D1 seawater reference materials. The concentrations of dFe measured in the SAFe reference samples were in good agreement with the consensus values (measured value,  $S = 0.12 \pm 0.04$  nM,  $n = 13$ ;  $D1 = 0.72 \pm 0.08$  nM,  $n = 14$ ; consensus value,  $S = 0.093 \pm 0.008$  nM;  $D1 = 0.67 \pm 0.04$ ).

Consensus values for dCo and dFe were reported to the GEO-TRACES Intercalibration Committee in 2010 (dCo) and 2011 (dFe), and are available at: <http://geotraces.org/science/intercalibration/322-standards-and-reference-materials>.

## 2.4. Nutrients, temperature, salinity and chlorophyll-*a*

Dissolved inorganic macronutrients, phosphate ( $\text{PO}_4^{3-}$ ) and nitrate ( $\text{NO}_2^- + \text{NO}_3^- = \Sigma \text{NO}_3$ ) were analysed on-board within 3–4 h of collection using a 5-channel segmented flow autoanalyser (Bran and Luebbe, AAI AutoAnalyzer) following standard colorimetric procedures (Grashoff et al., 1983) modified by Woodward et al. (1999). Low-level nutrients were not determined using liquid wave guides during AMT-19.

Salinity, temperature and dissolved  $\text{O}_2$  were measured using a CTD system (Seabird 911+). Dissolved  $\text{O}_2$  was determined by a Seabird SBE 43  $\text{O}_2$  sensor. Salinity was calibrated on-board using discrete samples taken from the OTE bottles using an Autosol 8400B salinometer (Guildline), whilst dissolved  $\text{O}_2$  was calibrated using

an automated photometric Winkler titration system (Carritt and Carpenter, 1966). Chlorophyll fluorescence and beam attenuation were determined using an Aquatraka MkIII fluorometer and Aquatraka MkII transmissometer (Chelsea Instruments), respectively. Sampling depths were determined by reference to the *in situ* fluorescence, temperature, salinity and irradiance (photosynthetically active radiation, PAR, 400–700 nm) profiles, to include 97%, 55%, 33%, 14%, 1% and 0.1% PAR levels. For chlorophyll-*a* determination, samples were filtered (0.2  $\mu\text{m}$  polycarbonate) and the filters extracted in 10 mL of 90 % acetone overnight at 4 °C (Welschmeyer, 1994). The chlorophyll-*a* extract was measured on a pre-calibrated (pure chlorophyll-*a* standard, Sigma-Aldrich) Turner Designs Trilogy 700 fluorimeter.

*Prochlorococcus* and *Synechococcus* were enumerated by flow cytometry using a Becton Dickinson FACSort (Oxford, UK) flow cytometer equipped with an air-cooled laser providing blue light at 488 nm (Tarran et al., 2006).

The trace metal (dCo, dFe and TdFe) data, ancillary data and a full station list are available at: <http://www.bodc.ac.uk/projects/uk/amt/>.

## 3. Results

### 3.1. Hydrographic setting and macronutrient distributions

The six biogeographical provinces used in this study are shown in Fig. 1. Note that the North Atlantic gyre is divided into two separate provinces; the North Atlantic subtropical gyre (NAST) and the North Atlantic tropical gyre (NATR). In these provinces, the thermohaline structure of the upper water column (Fig. 2) is primarily determined by the water masses that occupy each region and the relative evaporation and precipitation rates. In the North Atlantic, the lowest upper water column temperatures (12–22 °C) were observed in the NADR. Here, the water column displayed weak thermohaline stratification, characteristic of high wind stress in the NADR during boreal autumn (Longhurst, 1998).

In the NAST, the introduction of warmer (>20 °C), more saline (>36.5), water from the Gulf Stream enters via the Azores Current (AC, centred at 35–36°N) (Aiken et al., 2000) resulting in a mixed layer depth of between 40 and 50 m. Further south in the NATR, the North Equatorial Current (NEC, centred at 15°N) supplies water with salinity >37, due to the high rates of evaporation at these latitudes. Consistent with previous AMT observations (Aiken et al., 2000; Robinson, 2006), the NEC was observed to depths of ~150 m between 20 and 26°N during AMT-19.

Towards the southern extent of the NATR province, a plume of cooler (<20 °C), fresher (<36), lower oxygen (<150  $\mu\text{M}$ ) upwelled water was clearly visible below 60 m (Fig. 2). This oxygen minimum zone (OMZ), which extended throughout the tropical Atlantic to the southern boundary of the WTRA, results from the divergence between the North Equatorial Current (NEC) and the North Equatorial Counter Current (NECC) at ~10°N, and the divergence between the NECC and the South Equatorial Current (SEC) at ~2°S (Hastenrath and Merle, 1987; Longhurst, 1998; Aiken et al., 2000) (Fig. 1). Mixed layer depths (defined as the depth at which potential density differed by 0.05  $\text{kg m}^{-3}$  from the surface) in the WTRA varied between 9 and 95 m. Throughout the upper 150 m of the WTRA low salinity (<36.5) water, relative to the subtropical gyres, was observed caused by dilution through excess precipitation over evaporation (Aiken et al., 2000).

A surface salinity minimum (<35) was observed in the WTRA between ~6 and 10°N to a depth of 30 m (Fig. 2), a common feature that can arise from either converging air masses and subsequent high precipitation rates in the ITCZ, or from Amazon Water transported eastwards across the Atlantic by the NECC (Aiken et al.,

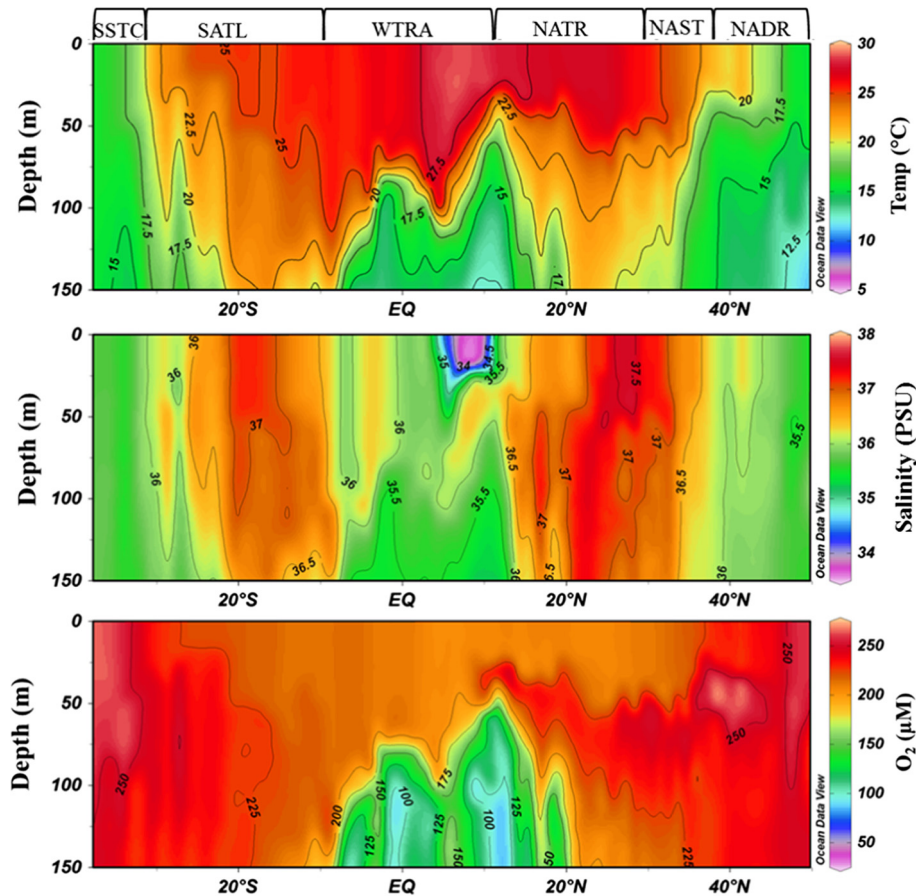


**Fig. 2.** The distributions of temperature (top), salinity (middle) and dissolved oxygen (bottom) in the upper 150 m of the Atlantic Ocean during AMT-19, with the biogeochemical provinces marked above (refer to Fig. 1 for acronyms). Stations were sampled approximately every 1–1.5° of latitude at a 1 m depth resolution.

2000). However, no elevation in surface silicate concentration (data not shown), which would be indicative of Amazon Water, was observed during AMT-19. In addition, two intense rainfall events were recorded between 6 and 9°N during the cruise, suggesting that the high rates of precipitation that characterise the ITCZ could be the cause of the WTRA salinity minimum.

As observed during earlier AMT studies (Robinson, 2006), a gradual latitudinal decrease in sea surface temperature and salinity was observed in the SATL (10–33°S) and into the SSTC (33–38°S), a manifestation of the decrease in evaporation rates associated with lower temperatures at higher latitudes. An increase in the westerly winds as the ship travelled south, coupled with increased downwelling associated with the anti-cyclonic circulation of the subtropical gyre (Longhurst, 1998; Ussher et al., 2013), resulted in a deepening of the SATL mixed surface layer down to 61 m, and a fully homogeneous upper water column ( $T \sim 16^\circ\text{C}$ ,  $S \sim 35.5$ ) in the SSTC.

The distribution of macronutrients along the transect (Fig. 3;  $\text{NO}_3$  data is not shown due to the similarity with the distribution of  $\text{PO}_4$ ) revealed extremely low mixed layer concentrations ( $\text{PO}_4 < 0.05 \mu\text{M}$ ) in the NAST and NATR and three distinct regions where concentrations below the mixed layer were elevated. Firstly, in the NADR, macronutrient concentrations were elevated below 60 m ( $\text{PO}_4 = 0.2\text{--}0.9 \mu\text{M}$ ,  $\text{NO}_3 = 2.5\text{--}12 \mu\text{M}$ ). These elevated concentrations continued into the northern section of the NAST before becoming depleted. Secondly, macronutrient concentrations were elevated in waters associated with the equatorial upwelling ( $\text{PO}_4 = 0.2\text{--}1.5 \mu\text{M}$ ,  $\text{NO}_3 = 2.5\text{--}23 \mu\text{M}$ ). Thirdly, macronutrient concentrations in the SSTC were elevated below 100 m ( $\text{PO}_4 = 0.2\text{--}$

$0.5 \mu\text{M}$ ;  $\text{NO}_3 = 2.5\text{--}5 \mu\text{M}$ ), values similar to those reported for the Southwest Atlantic at 40°S by Wyatt et al. (2014).

### 3.2. Dissolved Co and Fe distributions

Surface water (upper 25 m) dCo and dFe distributions during AMT-19 displayed distinct differences between the North and South Atlantic (Fig. 4). Surface dCo concentrations during AMT-19 were highly variable (10–93 pM). The lowest concentrations were observed in the northern gyre provinces (NAST  $25 \pm 14$  pM and NATR  $21 \pm 2.8$  pM, respectively,  $n = 6$ ), whilst higher concentrations were observed in the upwelling region (WTRA  $51 \pm 38$  pM,  $n = 9$ ) and the South Atlantic gyre (SATL  $60 \pm 31$  pM,  $n = 3$ ) (Fig. 4). This trend is similar to that previously reported for  $\text{PO}_4$ , with very low concentrations of  $\text{PO}_4$  (0.01–0.05  $\mu\text{M}$ ) observed in the North Atlantic gyre regions and higher concentrations (0.2–0.5  $\mu\text{M}$ ) in the South Atlantic gyre (Mather et al., 2008). At approximately 28°S the SATL is sub-divided into two cells separated by the subtropical counter-current. To the south of this front (25–30°S) the Brazil Current (BC) forms the southern extent of a recirculation cell (Mémery et al., 2000 and references therein). The high surface dCo in this region ( $89 \pm 4$  pM at 28.8°S, 26.1°W, Fig. 4) is attributed to offshore advection of continental Co mobilised by the western boundary current and a declining gradient is observed to the south of this frontal region.

The surface water (upper 25 m) dFe and TdFe distribution is in complete contrast to dCo, as dFe and TdFe were relatively high in the NATR and NAST, and low in the SATL (Fig. 4). The highest surface dFe and TdFe concentrations were observed in the NATR (dFe,

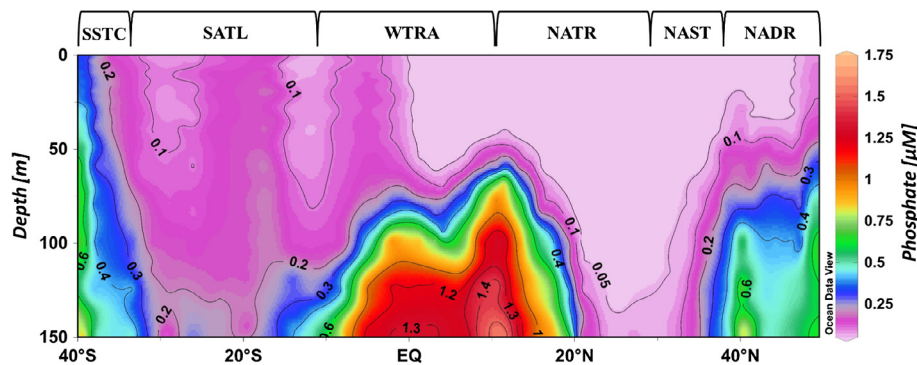


Fig. 3. Distribution of phosphate ( $\text{PO}_4$ ) in the upper 150 m of the Atlantic Ocean during AMT 19 with the biogeochemical provinces marked above (refer to Fig. 1 for acronyms). Note the higher concentrations in the SATL compared to the NAST and NATR.

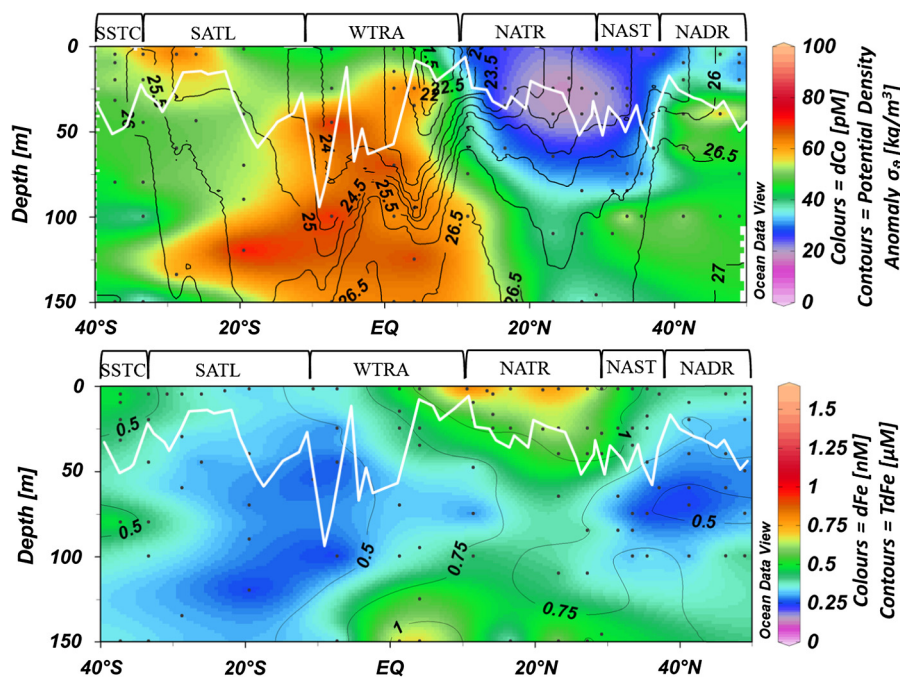


Fig. 4. The distribution of  $\text{dCo}$  (pM) overlaid with potential density anomaly ( $\text{kg m}^{-3}$ ; top panel),  $\text{dFe}$  (nM) overlaid with the  $\text{TdFe}$  (nM; bottom panel) in the upper 150 m of the Atlantic Ocean during AMT-19, with the approximate depth of the mixed layer marked (MLD) shown as a solid white line. The biogeochemical provinces are displayed above the top panel (refer to Fig. 1 for acronyms).

$0.68 \pm 0.28$  nM;  $\text{TdFe}$ ,  $1.1 \pm 0.25$  nM,  $n = 12$  and  $10$ , respectively) and the WTRA ( $\text{dFe}$ ,  $0.76 \pm 0.61$  nM;  $\text{TdFe}$   $1.3 \pm 0.33$  nM,  $n = 6$ ) provinces between  $\sim 5$  and  $30^\circ\text{N}$ , corresponding to the latitudinal extent of the Saharan plume ( $5$ – $30^\circ\text{N}$ ) (Prospero et al., 2002; Kaufman et al., 2005). Here, two distinct surface  $\text{dFe}$  maxima were observed. The first, located between  $\sim 20$  and  $28^\circ\text{N}$  ( $\text{dFe}$ ,  $0.88 \pm 0.14$  nM,  $n = 6$ ), was in the vicinity of the elevated rates of surface nitrogen fixation ( $0.85$ – $1.1$   $\text{nmol L}^{-1} \text{d}^{-1}$ ) determined during this study (data not shown, but available from [www.bodc.ac.uk](http://www.bodc.ac.uk)). The second, at  $\sim 10$ – $14^\circ\text{N}$  ( $0.74 \pm 0.58$  nM,  $n = 7$ ), overlapped with the ITCZ surface salinity minimum (Fig. 2), which is consistent with the observation that high rainfall rates associated with the ITCZ contributes to high wet deposition fluxes of Fe in the south NATR/north WTRA (Kim and Church, 2002; Powell et al., 2015). The locations of these two surface  $\text{dFe}$  maxima coincided with high  $\text{TdFe}$  concentrations ( $1.1 \pm 0.17$  nM and  $1.3 \pm 0.28$  nM, respectively) between  $4$  and  $30^\circ\text{N}$ , and are in excellent agreement with observations from previous North Atlantic studies (Bowie et al., 2002; Bergquist and Boyle, 2006; Measures et al., 2008; Ussher

et al., 2013). Combined with the low  $\text{dFe}$  in the SATL, the peaks in  $\text{dFe}$  and  $\text{TdFe}$  in the North Atlantic gyre provinces indicate the importance of atmospheric deposition in controlling surface  $\text{dFe}$  concentrations (e.g., Schlosser et al., 2013). North of  $\sim 30^\circ\text{N}$ , surface  $\text{dFe}$  concentrations were lower ( $0.34 \pm 0.14$  nM,  $n = 14$ ) and less variable (Fig. 4), most likely due to a reduced Saharan dust input and strong winter mixing in the NAST and NADR, compared with weak seasonal mixing in the NATR (Longhurst, 1998).

In sub-surface waters (deeper than 25 m), the  $\text{dCo}$  distribution was also a tale of sharp contrasts. Extremely low concentrations were observed throughout the North Atlantic gyre provinces, with the lowest concentrations ( $16 \pm 3.4$  pM,  $n = 8$ ) observed at the base of the mixed layer. The maximum abundances of *Prochlorococcus* ( $> 4 \times 10^5$  cells  $\text{mL}^{-1}$ ), a cyanobacteria with an absolute requirement for Co (Sunda and Huntsman, 1995a), in the North Atlantic gyre provinces were observed in the southern NATR in concert with a shoaling of the MLD, and were accompanied by very low  $\text{dCo}$  concentrations ( $13$ – $17$  pM at  $35$ – $40$  m depth), suggesting biological drawdown as an important control of  $\text{dCo}$  distribution in



this region. Higher dCo concentrations were observed in the provinces adjoining the northern gyre provinces, e.g., in the NADR (dCo =  $59 \pm 23$  pM,  $n = 10$ ) *Prochlorococcus* were less abundant and dCo appears to be advected southwards along the  $26 \text{ kg m}^{-3}$  isopycnal (Fig. 4, top panel) to  $\sim 40^\circ\text{N}$  and the boundary with the NAST.

The highest sub-surface dCo concentrations (e.g.  $89 \pm 4$  pM at  $28.8^\circ\text{S}$ ,  $26.1^\circ\text{W}$ ) were observed in the SATL. Between 25 and 150 m, the SATL was characterised by relatively high dCo ( $52 \pm 15$  pM,  $n = 10$ ), and decreasing temperature and salinity with increasing latitude. At the dynamic SATL/SSTC boundary ( $33.3^\circ\text{S}$ ,  $34.2^\circ\text{W}$ ), a slight increase in dCo was observed at 80 m relative to the surrounding water ( $58$  pM at 80 m,  $44$  pM at 45 m and  $29$  pM at 100 m). The source of this high dCo is not immediately clear, but may result from spin-off of eddies containing higher dCo water from the south. The presence of eddies in this region is confirmed by the sea surface anomaly image, Fig. S1 in the Supplementary Material. As concentrations of dCo can be highly variable over scales of  $\sim 10$  km (Saito and Moffett, 2002; Noble et al., 2008; Shelley et al., 2012), the low dCo observed at the adjoining station ( $15.5 \pm 0.3$  pM at  $35.3^\circ\text{S}$ ,  $37.1^\circ\text{W}$ ) may be just as characteristic of this province (reflecting seawater that has had no contact with the continental shelf and low atmospheric inputs) as water with high dCo. Regardless of the dCo concentration, in all gyre provinces dCo exhibited a broadly nutrient-type distribution (lower concentrations in the mixed layer than below it) in the upper 150 m.

The sub-surface distribution of dFe also displayed strong latitudinal gradients (Fig. 4). In a reversal of the trend for dCo, sub-surface dFe concentrations in the SATL were low and relatively uniform ( $0.26 \pm 0.06$  nM,  $n = 12$ ) compared with the northern gyre provinces ( $0.40 \pm 0.17$  nM,  $n = 25$ ) where atmospheric deposition is much higher. Below 100 m in the northern NATR/southern NAST waters between  $23$  and  $31^\circ\text{N}$ , the dFe and TdFe concentrations were  $0.48 \pm 0.14$  nM ( $n = 5$ ) and  $0.72 \pm 0.11$  nM ( $n = 5$ ), respectively and could be a relic of a previous atmospheric deposition event. Interestingly, we observed a similar feature at the same depth for dCo ( $36 \pm 3.4$  pM; Fig. 4).

For both dCo and dFe, elevated sub-surface concentrations were associated with the low oxygen waters. Maximum sub-surface dCo and dFe concentrations ( $62 \pm 16$  pM and  $0.62 \pm 0.20$  nM, respectively) were observed between  $0$  and  $10^\circ\text{N}$ , coincident with an oxygen minimum of  $100$ – $150$   $\mu\text{M}$  (Fig. 2). Observations of elevated dFe in this OMZ are consistent with previous studies (Bergquist and Boyle, 2006; Measures et al., 2008; Fitzsimmons et al., 2013; Ussher et al., 2013) suggesting that the elevated dFe may be a steady-state feature in this region, sustained by either remineralisation of high Fe:C organic matter formed in the Fe-rich surface and/or lateral mixing of high dFe water from sedimentary sources. However, in contrast to dFe, the elevated dCo concentrations were not confined to the OMZ, but extended over a broader latitudinal range (southwards) and wider depth range, suggesting that mechanisms other than remineralisation and low dissolved oxygen concentrations were sustaining the elevated dCo concentrations in this region.

#### 4. Discussion

Given that there are a number of similarities in the redox and organic speciation of Co and Fe, the difference in the distributions of these two elements in the Atlantic Ocean is stark. In the northern gyre provinces (NATR and NAST), where deposition and dissolution of atmospheric aerosols is the dominant source of Fe (e.g. Duce and Tindale, 1991; Duce et al., 1991; Sarthou et al., 2003; Jickells et al., 2005; Baker et al., 2006; Buck et al., 2010;

Evangelista et al., 2010; Ussher et al., 2013), the extremely low concentrations of dCo contrast strongly with the relatively high concentrations of dFe. A number of studies have alluded to an atmospheric source of Co which could influence surface dCo concentrations in regions of high atmospheric deposition (Bowie et al., 2002; Dulaquais et al., 2014a; Knauer et al., 1982; Thuroczy et al., 2010; Wong et al., 1995). Furthermore, aerosol Co is significantly more soluble than aerosol Fe (Dulaquais et al., 2014a; Mackey et al., 2015; e.g. 8–10% fractional solubility for Co and 0.44–1.1% fractional solubility for Fe for the same Saharan dust samples, Shelley et al., 2012), further supporting the assertion that atmospheric supply may play a pivotal role in controlling surface distributions of dCo and hence influence phytoplankton community dynamics.

For dFe, the sharpest gradient was observed at the NAST/NATR boundary, and is almost certainly linked to atmospheric inputs and the approximate location of the northern extent of the Saharan plume. Indeed the relationship between dFe in the upper water column and atmospheric supply are well documented (e.g. Bowie et al., 2002; Baker et al., 2006, 2007, 2013; Rijkenberg et al., 2012; Ussher et al., 2013), which makes the low dCo in the same latitudinal band somewhat of a paradox. One explanation could be that the Co is being scavenged in the water column following oxidation by manganese (Mn) oxidising bacteria, which oxidise both Mn and Co via a common microbial pathway (Moffett and Ho, 2001). However, significant removal via the Mn co-oxidation pathway is not supported by the literature in open ocean environments, as it is driven by competitive inhibition (Moffett and Ho, 1996; Noble et al., 2012) and dCo is low (this study; Noble, pers. comm.) and dMn is high (Wu et al., 2014; Hatta et al., 2014) in the northern gyre provinces.

In the vicinity of the ITCZ, both dFe and TdFe were significantly inversely related to salinity in the mixed layer ( $r^2 = 0.89$  and  $0.82$  respectively;  $p < 0.05$ ,  $n = 5$ ) suggesting that the scavenging of dust incursions into the ITCZ (Adams et al., 2012) as it migrated south towards to its boreal winter position (centred at  $\sim 5^\circ\text{N}$ ) could be a source of Fe to surface waters at the NATR/WTRA border, as described by Kim and Church (2002). However, the small number of samples ( $n = 5$ ) make any links tenuous at best, particularly as this relationship is driven by the high dFe and TdFe values (both  $1.1$  nM) at  $1.5$  m depth at  $10.6^\circ\text{N}$ ,  $32.0^\circ\text{W}$ . Similarly, the relatively sparse dCo dataset for mixed layer waters influenced by the ITCZ ( $n = 4$ ) makes assessing a link between dCo and precipitation unrealistic, and is further complicated by the limited literature on dCo in rainwater of the ITCZ and the contrasting conclusions reached; i.e. either precipitation dilutes surface dCo (Helmerts and Schrems, 1995; Pohl et al., 2010), or it is a source of dCo (Bowie et al., 2002). In this study, two modest enrichments of dCo (relative to the underlying water and to adjoining stations) coincided with rain events at  $\sim 31^\circ\text{N}$ , and the intense rain events in the ITCZ at  $6$  and  $9^\circ\text{N}$  (Chieze, pers. Comm; <http://www.giovanni.sci.gsfc.nasa.gov>). At  $31^\circ\text{N}$ , for example, the concentration of dCo was  $46.4$  pM at  $2$  m depth, whereas at  $25$  m depth dCo had been drawn down to  $21.2$  pM. In addition, wet deposition has been estimated to account for  $>90\%$  of the total atmospheric deposition flux of Co, compared with just  $20\%$  for Fe, based on data from Bermuda (Church, unpublished data). In the eastern tropical Atlantic (in September–November), Powell et al. (2015) estimate that wet deposition may be a relatively more important source of Fe than in the western North Atlantic gyre, contributing up to  $70\%$  of the total atmospheric flux.

We have estimated the soluble Co and Fe deposition fluxes for  $20^\circ\text{N}$  and  $20^\circ\text{S}$  from dry deposition data published in Shelley et al. (2015) and Dulaquais et al. (2014a) ( $20^\circ\text{N}$ ) and Chance et al. (2015) ( $20^\circ\text{S}$ ) (Table 1). For Co, in the NATR, under the Saharan outflow, dry deposition contributes only  $1.4\%$  of the mixed

layer depth (MLD) concentration of dCo (assuming permanent stratification of the water column). In contrast, atmospheric deposition may supply twice the amount of dFe observed in the mixed layer over the course of the year. In the SATL, where atmospheric deposition may be orders of magnitude lower, atmospheric supply alone cannot account for the concentrations of either metal observed ( $\ll 0.5\%$  and  $21\%$  of mixed layer dCo and dFe, respectively). It is noted that these atmospheric deposition fluxes do not account for wet deposition, and thus, the estimates presented in Table 1 may be rather conservative. Nonetheless, these data highlight the role of atmospheric deposition in controlling the dFe concentrations in surface waters of the two gyre regions. For Co, the impact of atmospheric deposition is more subtle.

Our calculations are sensitive to the percentage of the metal that is soluble in seawater. Unfortunately, aerosol metal solubility is poorly constrained. In Table 1, a Co solubility value of  $9.0\%$  is used for the NATR (Dulaquais et al., 2014a). However, Co solubility is a function of the composition of the bulk aerosol, which in turn is a function of aerosol provenance, and may be up to threefold higher (i.e.,  $\sim 30\%$ , Shelley, unpublished data, available at: [www.bco-dmo.org](http://www.bco-dmo.org)) in aerosols sourced from Europe as opposed to those from North Africa, due to a higher component of industrial emission aerosols in the former. This will result in a higher flux of soluble Co, and given the extremely low concentrations of dCo in the northern gyre provinces, suggests that atmospheric supply may still have an important role in supplying Co to surface waters (Thuroczy et al., 2010).

If, as our data suggests, aerosols are indeed a source of Co to the northern gyre provinces, how can the contrasting distributions of dCo and dFe be reconciled? We hypothesise that biological uptake primarily by the dominant components of the bacterial assemblage, such as the cyanobacteria *Prochlorococcus* and *Trichodesmium*, is exceeding supply, leading to a dCo deficit in the northern gyre provinces (NAST, NATR).

#### 4.1. Biological controls on dissolved Co distributions

Although *Prochlorococcus* are ubiquitous in tropical and subtropical oceans, their range extends throughout the Atlantic from  $\sim 50^\circ\text{N}$  to  $40^\circ\text{S}$  (Heywood et al., 2006). *Prochlorococcus* thrive in oligotrophic conditions and have an obligate requirement for Co for carbon fixation (Sunda and Huntsman, 1995a; Saito et al., 2002). During AMT-19, *Prochlorococcus* dominated the picoplankton assemblage, with *Synechococcus* only proliferating where *Prochlorococcus* abundance was less than  $10^5$  cells  $\text{mL}^{-1}$  (Fig. 5), i.e., the temperate margins of this AMT transect (NADR and SSTC), and in the low-salinity ( $<35$ ) surface waters of the ITCZ (upper 30 m at  $6\text{--}10^\circ\text{N}$ ; Fig. 2). Our data are consistent with the observation that *Prochlorococcus* typically outnumber *Synechococcus* by one to two orders of magnitude in stratified, oligotrophic waters (Durand et al., 2001).

In this study, the highest abundances of *Prochlorococcus* were observed in the high-dCo tropical upwelling region ( $\sim 5^\circ\text{N}$  to  $5^\circ\text{S}$ ) (Fig. 5). This contrasts with the phytoplankton dynamics in another high dCo upwelling region, the Costa Rica upwelling dome (CRD), where *Synechococcus* dominated the picoplankton assemblage (Ahlgren et al., 2014).

In terms of *Prochlorococcus* abundance, the northern gyre was divided in two (at approximately the boundary between the NATR and NAST). The NAST and NATR, were both characterised by extremely low dCo concentrations, with the dCo minima (NAST =  $15 \pm 3.8$ , NATR =  $15 \pm 1.4$  pM, at  $28\text{--}45$  m) generally corresponding with the maximum abundances of *Prochlorococcus* in these provinces (Fig. 5). The *Prochlorococcus* maxima were at shallower depths than the DCM (e.g.,  $4 \times 10^5$  cells  $\text{mL}^{-1}$  at  $29$  m at  $11.5^\circ\text{N}$ , compared to a DCM of  $0.41 \mu\text{g L}^{-1}$  chl-*a* between  $46$  and

$50$  m). The relationship between dCo distributions, *Prochlorococcus* abundance, and the relative position of the DCM has previously been observed in the Sargasso Sea (western NAST/NATR; Shelley et al., 2012).

In the NATR, *Prochlorococcus* abundance was high ( $>3 \times 10^5$  cells  $\text{mL}^{-1}$ ), even though dCo was extremely low ( $22 \pm 15$  pM). In the NAST, dCo was similarly low ( $22 \pm 3.8$  pM), but *Prochlorococcus* abundance was lower than in the NATR (generally  $<2 \times 10^5$  cells  $\text{mL}^{-1}$ ). As atmospheric deposition decreases northwards from the NATR to NAST, we hypothesise that aerosol supply indirectly impacts *Prochlorococcus* abundance via its role as a key source of Co and Fe. Moreover, the sub-surface dCo minimum coincides with the region of maximum rates of nitrogen fixation during AMT-19 ( $21\text{--}23^\circ\text{N}$ ), consistent with a Co requirement for nitrogen fixation by *Trichodesmium* (Rodriguez and Ho, 2015), which are abundant in the tropical to subtropical North Atlantic, but almost entirely absent between  $5$  and  $30^\circ\text{S}$  (Tyrrell et al., 2003; Schlosser et al., 2013). In the SATL, dCo concentrations and *Prochlorococcus* abundance were decoupled to the extent that the opposite trend was observed, with high dCo and high abundances of *Prochlorococcus* occurring together. This occurred in concert with a near absence of *Trichodesmium*, suggesting that the presence/absence of *Trichodesmium* may also have an important role in driving the dCo distribution.

Moreover, the presence/absence of other bacteria may influence dCo distributions. Although the bacterial abundance was roughly equivalent in the SATL and NATR/NAST during AMT-19 (M. Zubkov, pers. comm.) differences in the bacterial community composition have been reported between the two gyres (Schattenhofer et al., 2009; Friedline et al., 2012). In addition to the cyanobacteria, the marine bacteria SAR11, require Co for vitamin B<sub>12</sub> (Carini et al., 2013) and are more abundant in the northern gyre provinces and WTRA compared to the SATL (Schattenhofer et al., 2009, 2011; Friedline et al., 2012). Recent work has demonstrated that bacteria are the first to directly respond to Saharan dust inputs of trace elements and nutrients, and these authors argue that the bacterial assemblage is a key mediator of trace metal distributions following dust deposition (Westrich et al., 2016). Thus, the differences in bacterial community composition can impact the biogeochemical cycle of Co and hence explain the differing dCo distributions between the northern and southern gyres.

In addition to active uptake, *Trichodesmium*, which are abundant in the subtropical/tropical North Atlantic due to the delivery of atmospheric Fe (Richier et al., 2012) and P (Ridame et al., 2003), can scavenge both Fe (Rubin et al., 2011) and P from solution (Sanudo-Wilhelmy et al., 2001). Could the same removal mechanism be an important sink for Co? Although we do not have particulate Co or TdCo data for AMT-19, TdCo was determined in surface samples (7 m depth) on AMT-3 (a similarly gyre-centred AMT; Bowie et al., 2002), where low concentrations of  $\sim 30$  pM dCo (AMT-19) and TdCo (AMT-3) were observed between  $3$  and  $17^\circ\text{N}$ . In addition, recent studies of particulate Co in the Atlantic Ocean, demonstrated that it was  $\sim 5\%$  the concentration of dCo in a full-depth transect along  $\sim 12^\circ\text{S}$  (Noble et al., 2012) and  $12 \pm 12$  in the West Atlantic (Dulaquais et al., 2014a), suggesting that scavenging may only be a minor sink for Co under a range of open ocean environmental conditions.

Lastly, dCo distributions can be influenced by dissolved organic phosphorus (DOP) acquisition. The region where extremely low dCo was observed is also where chronically low PO<sub>4</sub> concentrations are observed (Mather et al., 2008). In the North Atlantic gyre provinces the DOP pool is 5–10 times higher than inorganic phosphorus and phytoplankton and bacteria must utilise AP to acquire their essential phosphorus requirement (Mahaffey et al., 2014). Zinc is the metal co-factor in the protein PhoA used for AP activity and, while Co can substitute for Zn as the metal centre in PhoA



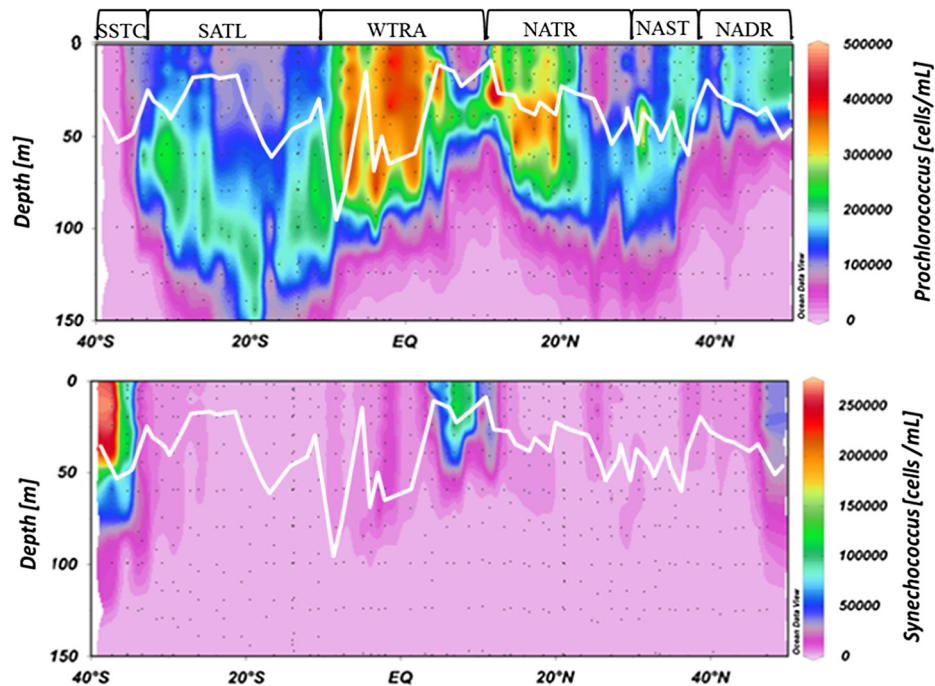


Fig. 5. *Prochlorococcus* and *Synechococcus* distributions in the upper 150 m during AMT-19. The white line depicts the approximate depth of the mixed layer.

(Sunda and Huntsman, 1995a), the preference is for Zn (Saito and Goepfert, 2008). A recent study in the sub-tropical Atlantic has demonstrated that Zn concentrations, which are very low in this region, could limit AP activity (Mahaffey et al., 2014). Therefore, the low Co concentrations may arise from uptake by cyanobacteria and also from its substitution for Zn in AP. Using Co uptake results from freshwater phytoplankton grown under  $PO_4$  limitation, Ji and Sherrell (2008) hypothesised, that the very high demand for Co in the tropical North Atlantic may be the result of persistent  $PO_4$  stress in this region. However, the discovery of a calcium (Ca)-based AP (Kathuria and Martiny, 2011) suggests that at least some *Prochlorococcus* ecotypes and bacteria are able to bypass the need for Co in AP, which may reduce the potential for Co-Zn-P co-limitation. However, field based evidence in this region clearly shows that the AP activity is limited by Zn (Mahaffey et al., 2014) as a result of the extremely low dZn concentrations in the North Atlantic (Conway and John, 2014; Roshan and Wu, 2015) and with the low dCo concentrations observed in this study AP activity may also be limited by Co

In the SATL, *Trichodesmium* is largely absent (Tyrrell et al., 2003; Schlosser et al., 2013), and *Prochlorococcus* abundance was lower, with maximum abundances deeper than in the northern gyre provinces likely due to significantly lower dFe concentrations, and a deeper MLD in the northern section of the SATL compared with the NATR/NAST (Figs. 4 and 5). The positive correlations between dCo and *Prochlorococcus* abundance in the South Atlantic (Fig. S2, Supplemental Material) may be linked with higher inorganic phosphorus availability, as well as higher dCo. In the South Atlantic, where atmospheric deposition is low, a combination of highly efficient internal cycling (85% of the dCo uptake rate in the SATL may be accounted for by remineralisation of organic matter, Dulaquais et al., 2014a), lateral inputs (Bown et al., 2011; Noble et al., 2012) and relatively low biological demand results in higher dCo concentrations compared with the northern gyre provinces.

The different relationship between dCo and bacterial dynamics in the northern gyres and the SATL suggests that dCo availability has the potential to influence both the bacterial and phytoplankton community structure, or vice versa, through a complex interplay

with other factors, such as Fe and inorganic phosphorus availability. However, the northern gyre provinces appear unique in the sense that biotic removal dominates and controls dCo distributions (Moffett and Ho, 1996). In future decades increased stratification and predicted increases in nitrogen supply (Behera et al., 2013) could exacerbate the disparity between the northern and southern gyres in terms of trace metal distributions as a result of proximal nutrient limitation and, thus, the potential for changes to the bacterioplankton community structure.

#### 4.2. Low oxygen waters

Upwelling (vertical transport) can deliver macro- and micronutrient-enriched deep water to the mixed layer of the tropical North Atlantic, although for Fe the dominant flux is from the atmosphere (Ussher et al., 2013). Using the average dCo and dFe concentrations from below the surface mixed layer of the WTRA during AMT-19 (64 and 421  $nmol\ m^{-3}$ , respectively) and an upward vertical mixing rate of 14.3  $m\ y^{-1}$  (based on the method presented by Ussher et al. (2013) for a similar cruise track, AMT-16), we estimate an upward vertical mixing flux of 2.5 and 16.5  $nM\ m^{-2}\ d^{-1}$  for dCo and dFe, respectively. The combination of this upward vertical transport of nutrient-rich water and atmospheric supply sustains relatively high algal biomass in surface waters of the tropical Atlantic (e.g., the maximum chl-*a* concentration of 0.41  $\mu g\ L^{-1}$  was observed at 11.5 N at 46–50 m just above the thermocline and oxycline). These high levels of primary productivity result in a large amount of sinking detritus. Bacterial degradation of this detritus consumes oxygen which, in turn, contributes to the development of OMZs. In the productive eastern equatorial Atlantic, a broad OMZ extends from ~100 to 900 m depth (Karstensen et al., 2008).

Both high dCo and dFe have previously been reported in the oxygen deficient waters of the WTRA (Bowie et al., 2002; Measures et al., 2008; Pohl et al., 2010) and during AMT-19 elevated dCo (>60 pM) and dFe (>0.60 nM) were observed in the OMZ of the WTRA. However, while elevated dFe in the sub-surface WTRA was associated with the OMZ (150  $\mu M$  contour posi-

tioned at depths >40–100 m depending on latitude), elevated subsurface dCo covered a much wider depth range and was not confined to the WTRA, spilling over into the SATL at depths below ~100 m (Fig. 4). It is unlikely that the WTRA is supplying dCo to the SATL, as the two provinces are separated by the South Equatorial Current (SEC), and there is no evidence of elevated dFe to the south of the upwelling zone. Rather, preferential scavenging of Fe with respect to Co, in the Benguela and South Equatorial Currents (Noble et al., 2012), which feed into the South Atlantic gyre, provides the most likely explanation for the difference in dCo and dFe concentrations to the south of the upwelling zone.

During AMT-19, the 100  $\mu\text{M}$   $\text{O}_2$  contour was observed to shoal to depths as shallow as 100 m, and in the WTRA as a whole the DCM was positioned just above the 150  $\mu\text{M}$   $\text{O}_2$  horizon. In these productive waters bacterial degradation of sinking organic particles is evidenced by the apparent oxygen utilisation (AOU). Furthermore, the bacteria that consume the oxygen during the bacterial degradation of particles may be an additional source of high-affinity, metal binding ligands (Barbeau et al., 2001, 2003) which also retain remineralised Co and Fe in solution. While a positive relationship between dFe and AOU ( $r^2 = 0.6$ ,  $p = 0.03$ ,  $n = 7$ ) in the latitudinal band 1–17°N, was observed, for dCo and AOU the relationship was weak and not significant ( $r^2 = 0.2$ ,  $p = 0.3$ ,  $n = 8$ ) (Fig. 6), suggesting that other sources of Co (e.g., vertical transport, lateral advection) are relatively more important in this region.

#### 4.3. Lateral transport

In this study, surface dFe concentrations in the NADR of 0.20–0.58 nM were similar to the 0.14–0.60 nM reported by Ussher et al. (2007) for Northeast Atlantic surface waters. These authors observed a dFe concentration gradient over a relatively short distance spanning the shelf break, and concluded that minimal lateral transport of dFe from the shelf to the open ocean occurred in this region, despite severe winter storms. In this study, there was little evidence for the lateral transport of dFe from the European shelf margin to the open ocean. In contrast, in the NADR, a sharp gradient in dCo was observed at the boundary with the NAST with the highest concentrations of dCo appearing to be transported offshore along the 26.0  $\text{kg m}^{-3}$  isopycnal. In the South Atlantic, although the Falkland/Malvinas Current could potentially be a vector for the offshore transport of dFe, here, too, we saw no evidence for the offshore transport of dFe.

Lateral advection may however, be a more important source of dCo. Indeed, Bown et al. (2011) report evidence of just such a mechanism in the Southeast Atlantic Ocean. Furthermore, Noble et al. (2012) also observed a large-scale (>2000 km), offshore dCo

plume in the SATL. These authors also noted offshore advection of dFe, but that the plume covered a far smaller distance (<500 km) than the dCo plume, and despite no evidence for offshore advection of dMn (a tracer for sedimentary inputs), they concluded that reducing sediments on the African margin were a likely source of all three metals. However, dFe and dMn were scavenged preferentially to dCo, which explained the difference in the extent of the offshore plumes. Dulaquais et al. (2014b) also argue that scavenging is a fairly insignificant removal term for dCo in the western Atlantic, as they were unable to resolve dCo removal, via scavenging, from dilution by mixing.

To the south of the SATL, the cruise track passed through a dynamic frontal region, the confluence of the Brazil and the Falkland/Malvinas Currents. Both western boundary currents flow along the continental shelf until they meet and are deflected offshore. Indeed, Boebel et al. (1999) and Jullion et al. (2010) report cross frontal mixing in the Argentine Basin of the subtropical surface waters of the Brazil Current and sub-Antarctic Surface Water from the Southern Ocean at the Brazil- Falkland/Malvinas confluence. Furthermore, as only about 3% of fluvial Co is estimated to be retained within river systems (Sholkovitz and Copland, 1981), the northward flowing Falkland/Malvinas Current may also transport organically-complexed fluvial Co offshore, contributing to the elevated surface concentrations in this frontal region, as has previously been reported for Fe (Rijkenberg et al., 2014).

#### 5. Conclusions

Dissolved Co and Fe distributions showed strong, and often contrasting, regional differences during AMT-19. Extremely low concentrations of dCo (NATR/NAST; ~20–30 pM) were observed in the northern gyre provinces where dFe was high, whereas the opposite trend was observed in the SATL. Both dCo and dFe distributions were generally nutrient-like; highlighting the nutritive role of these two bioactive elements. However, the extremely low dCo of the northern gyre provinces is somewhat of a paradox given the seemingly plentiful supply of trace elements from Saharan dust. In these regions, we propose that dCo distribution in waters shallower than ~100 m is controlled predominantly by biological uptake by the bacteria (primarily *Prochlorococcus*, *Trichodesmium* and SAR11), and other organisms that utilise a Co analogue of AP for DOP uptake. This has important implications in the context of climate change, where stratification is predicted to increase, thus reducing phosphate inputs from below to surface waters. This situation may be further exacerbated by predicted increases in nitrogen deposition (Behera et al., 2013) as a result

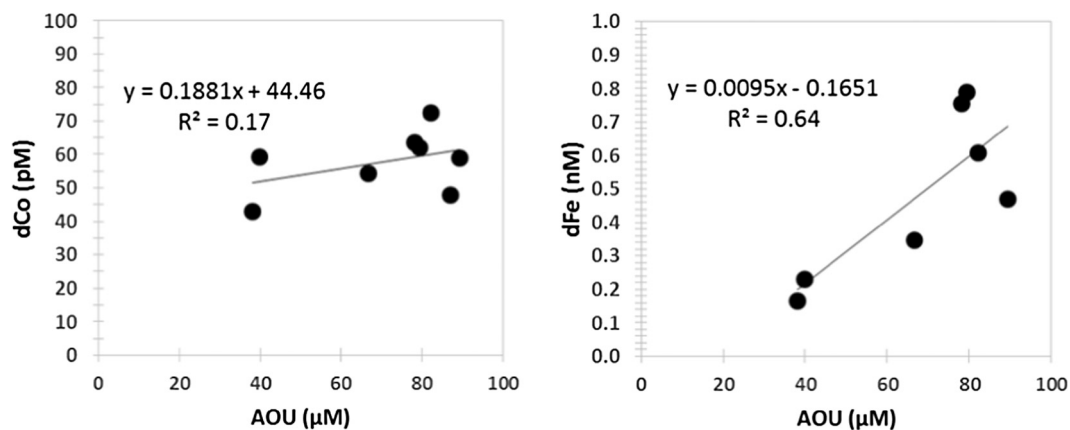


Fig. 6. dCo (left) and dFe (right) plotted against the apparent oxygen utilisation (AOU;  $\mu\text{M}$ ) in the region of low dissolved oxygen (>150  $\mu\text{M}$  dissolved oxygen; 1–17°N).

of increasing urbanisation/ industrialisation. Future studies should assess the potential for Co-Zn-P limitation in the North Atlantic.

## Acknowledgements

With many thanks to the Captain and crew of RRS James Cook, and Carolyn Harris, Malcolm Woodward and Claire Widdicombe for kindly providing the nutrient, and the chl-*a* data, respectively. Thank you also to Mike Zubkov and Manuela Hartmann for discussion of bacterial abundance during AMT-19. We thank two anonymous reviewers for their valuable comments and suggestions. Funding for this work was provided through a Marine Institute (Plymouth University), UK Studentship to RUS, a Natural Environment Research Studentship (NERC) to NJW and NERC grant number NE/G016267/1 to MCL. Thank you also to the Atlantic Meridional Transect Programme co-ordinators who provided a berth on AMT-19 and therefore made this study possible. This study is a contribution to the international IMBER project and was supported by the UK NERC National Capability funding to Plymouth Marine Laboratory and the National Oceanography Centre, Southampton. This is contribution number 277 of the AMT programme.

## Appendix A. Supplementary material

Supplementary data associated with this article can be found, in the online version, at <http://dx.doi.org/10.1016/j.pocan.2016.10.013>.

## References

- Adams, A.M., Prospero, J.M., Zhang, C., 2012. CALIPSO-derived three-dimensional structure of aerosol over the Atlantic basin and adjacent continents. *J. Clim.* 25, 6862–6879.
- Ahlgren, N.A. et al., 2014. The unique trace metal and mixed layer conditions of the Costa Rica upwelling dome support a distinct and dense community of *Synechococcus*. *Limnol. Oceanogr.* 59, 2166–2184.
- Aiken, J. et al., 2000. The Atlantic Meridional Transect: overview and synthesis of data. *Prog. Oceanogr.* 45, 257–312.
- Baars, O., Croot, P.L., 2015. Dissolved cobalt speciation and reactivity in the eastern tropical North Atlantic. *Mar. Chem.* 173, 310–319.
- Baker, A.R., Adams, C., Bell, T.G., Jickells, T.D., Ganzeveld, L., 2013. Estimation of atmospheric nutrient inputs to the Atlantic Ocean from 50N to 50S based on large-scale filed sampling: iron and other dust-associated elements. *Global Biogeochem. Cycles* 27, 755–767.
- Baker, A.R., Jickells, T.D., Witt, M., Lings, K.L., 2006. Trends in the solubility of iron, aluminium, manganese and phosphorus in aerosol collected over the Atlantic Ocean. *Mar. Chem.* 98, 43–58.
- Baker, A.R., Weston, K., Kelly, S.D., Voss, M., Streu, P., Cape, J.N., 2007. Dry and wet deposition of nutrients from the tropical Atlantic atmosphere: links to primary productivity and nitrogen fixation. *Deep Sea Res. Part I* 54, 1704–1720.
- Barbeau, K., Rue, E.L., Bruland, K.W., Butler, A., 2001. Photochemical cycling of iron in the surface ocean mediated by microbial iron(III)-binding ligands. *Nature* 413, 409–413.
- Barbeau, K., Rue, E.L., Trick, C.G., Bruland, K.W., Butler, A., 2003. Photochemical reactivity of siderophores produced by marine heterotrophic bacteria and cyanobacteria based on characteristic Fe(III) binding groups. *Limnol. Oceanogr.* 48, 1069–1078.
- Behera, S.N., Sharma, M., Aneja, V.P., Balasubramanian, R., 2013. Ammonia in the atmosphere: a review on emission sources, atmospheric chemistry and deposition on terrestrial bodies. *Environ. Sci. Poll. Res.* 20, 8092–8131.
- Bergquist, B.A., Boyle, E.A., 2006. Dissolved iron in the tropical and subtropical Atlantic Ocean. *Global Biogeochem. Cycles* 20. <http://dx.doi.org/10.1029/2005GB002505>.
- Bertrand, E.M. et al., 2007. Vitamin B<sub>12</sub> and iron co-limitation of phytoplankton growth in the Ross Sea. *Limnol. Oceanogr.* 52, 1079–1093.
- Blain, S. et al., 2007. Effect of natural iron fertilisation on carbon sequestration in the Southern Ocean. *Nature* 446, 1070–1074.
- Boebel, O., Schmid, C., Zenk, W., 1999. Kinematic elements of Antarctic Intermediate Water in the western South Atlantic. *Deep Sea Res. Part II* 46, 355–392.
- Bonnet, S., Webb, E.A., Panzeca, C., Karl, D.M., Capone, D.G., Sanudo-Wilhelmy, S.A., 2010. Vitamin B<sub>12</sub> excretion by cultures of the marine cyanobacteria *Crocosphaera* and *Synechococcus*. *Limnol. Oceanogr.* 55. <http://dx.doi.org/10.4319/lo.2010.55.5.1959>.
- Bowie, A.R., Whitworth, D.J., Achterberg, E.P., Mantoura, R.F.C., Worsfold, P.J., 2002. Biogeochemistry of Fe and other trace elements (Al, Co, Ni) in the upper Atlantic Ocean. *Deep Sea Res. Part I* 49, 605–636.
- Bown, J. et al., 2011. The biogeochemical cycle of dissolved cobalt in the Atlantic and the Southern Ocean south off the coast of South Africa. *Mar. Chem.* 126, 193–206.
- Boyd, P.W., Ellwood, M.J., 2010. The biogeochemical cycle of iron in the ocean. *Nat. Geosci.* 3, 675–682.
- Boyd, P.W. et al., 2007. Mesoscale iron enrichment experiments 1993–2005: synthesis and future directions. *Science* 315, 612–617.
- Browning, T.J., Bouman, H.A., Moore, C.M., Schlosser, C., Tarran, G.A., Woodward, E. M.S., Henderson, G.M., 2014. Nutrient regimes control phytoplankton ecophysiology in the South Atlantic. *Biogeosciences* 11, 463–479.
- Bruland, K.W., Lohan, M.C., 2003. Controls of trace metals in seawater. In: Elderfield, H. (Ed.), *The Oceans and Marine Geochemistry, Treatise on Geochemistry*, vol.6. Elsevier, Oxford, pp. 23–47.
- Buck, C.S., Landing, W.M., Resing, J.A., Measures, C.I., 2010. The solubility and deposition of aerosol Fe and other trace elements in the North Atlantic Ocean: observations from the A16N CLIVAR/CO<sub>2</sub> repeat hydrography section. *Mar. Chem.* 120, 57–70.
- Buck, K.N., Sohst, B., Sedwick, P.N., 2015. The organic complexation of dissolved iron along the U.S. GEOTRACES (GA03) North Atlantic Section. *Deep Sea Res. II* 116, 152–165.
- Carini, P., Steindler, L., Beszteri, S., Giovannoni, S.J., 2013. Nutrient requirements for growth of the extreme oligotroph 'Candidatus Pelagibacter ubique' HTCC1062 on a defined medium. *ISME J.* 7, 592–602.
- Carritt, D.E., Carpenter, J.H., 1966. Comparison and evaluation of currently employed modifications of the Winkler method for determining dissolved oxygen in seawater; a NASCO Report. *J. Mar. Res.* 24, 286–319.
- Chance, R., Jickells, T.D., Baker, A.R., 2015. Atmospheric trace metal concentrations, solubility and deposition fluxes in remote marine air over the south-east Atlantic. *Mar. Chem.* <http://dx.doi.org/10.1016/j.marchem.2015.06.028>.
- Conway, T.M., John, S.G., 2014. The biogeochemical cycling of zinc and zinc isotopes in the North Atlantic Ocean. *Global Biogeochem. Cycles* 28, 1111–1128.
- Coale, K.H. et al., 1996. A massive phytoplankton bloom induced by an ecosystem-scale iron fertilization experiment in the equatorial Pacific Ocean. *Nature* 383, 495–501.
- Croft, M.T., Lawrence, A.D., Raux-Deery, E., Warren, M.J., Smith, A.G., 2005. Algae acquire vitamin B<sub>12</sub> through a symbiotic relationship with bacteria. *Nature* 438, 90–93.
- Croot, P.L., Heller, M.I., 2012. The importance of kinetics and redox in the biogeochemical cycling of iron in the surface ocean. *Front. Microbiol.* 3. <http://dx.doi.org/10.3389/fmicb.2012.00219>.
- Croot, P.L., Streu, P., Baker, A.R., 2004. Short residence time for iron in surface seawater impacted by atmospheric dry deposition from Saharan dust events. *Geophys. Res. Lett.* 31. <http://dx.doi.org/10.1029/2004gl020153>.
- Cruz-López, R., Maske, H., 2016. The vitamin B<sub>1</sub> and B<sub>12</sub> required by themarine dinoflagellate *Lingulodinium polyedrum* can be provided by its associated bacterial community in culture. *Front. Microbiol.* 7. <http://dx.doi.org/10.3389/fmicb.2016.00560>.
- de Baar, H.J.W. et al., 2008. Titan: A new facility for ultraclean sampling of trace elements and isotopes in the deep oceans in the international GEOTRACES program. *Mar. Chem.* 111, 4–21.
- Doherty, O.M., Riemer, N., Hameed, S., 2012. Control of Saharan mineral dust transport to Barbados in winter by the Intertropical Convergence Zone over West Africa. *J. Geophys. Res. Atmos.* 117. <http://dx.doi.org/10.1029/2012JD017767>.
- Doherty, O.M., Riemer, N., Hameed, S., 2014. Role of the convergence zone over West Africa in controlling Saharan mineral dust load and transport in the boreal summer. *Tellus B* 66. <http://dx.doi.org/10.3402/tellusb.v66.23191>.
- Donat, J.R., Bruland, K.W., 1988. Direct determination of dissolved cobalt and nickel in seawater by differential pulse cathodic stripping voltammetry preceded by adsorptive collection of cyclohexane-1,2-dione dioxime complexes. *Anal. Chem.* 60, 240–244.
- Duce, R.A. et al., 1991. The atmospheric input of trace species to the world ocean. *Global Biogeochem. Cycles* 5, 193–259.
- Duce, R.A., Tindale, N.W., 1991. Atmospheric transport of iron and its deposition to the ocean. *Limnol. Oceanogr.* 36, 1715–1736.
- Dulaquais, G. et al., 2014a. Contrasting biogeochemical cycles of cobalt in the surface western Atlantic Ocean. *Global Biogeochem. Cycles* 28. <http://dx.doi.org/10.1002/2014GB004903>.
- Dulaquais, G., Boye, M., Rijkenberg, M.J.A., Carton, X., 2014b. Physical and remineralization processes govern the cobalt distribution in the deep western Atlantic Ocean. *Biogeosciences* 11, 1561–1580.
- Durand, M.D., Olson, R.J., Chisholm, S.W., 2001. Phytoplankton population dynamics at the Bermuda Atlantic time-series station in the Sargasso Sea. *Deep Sea Res. II* 48, 1983–2003.
- Ellwood, M.J., van den Berg, C.M.G., 2001. Determination of organic complexation of cobalt in seawater by cathodic stripping voltammetry. *Mar. Chem.* 75, 33–47.
- Evangelista, H. et al., 2010. Inferring episodic atmospheric iron fluxes in the western South Atlantic. *Atmos. Environ.* 44, 703–712.
- Fitzsimmons, J.N., Zhang, R., Boyle, E.A., 2013. Dissolved iron in the tropical North Atlantic Ocean. *Mar. Chem.* 154, 87–99.
- Friedline, C.J., Franklin, R.B., McCallister, S.L., Rivera, M.C., 2012. Bacterial assemblages of the eastern Atlantic Ocean reveal both vertical and latitudinal biogeographic signatures. *Biogeosciences* 9, 2177–2193.



- Gong, N., Chen, C., Xie, L., Chen, H., Lin, X., Zhang, R., 2005. Characterization of a thermostable alkaline phosphatase from a novel species *Thermus yunnanensis* sp. nov. and investigation of its cobalt activation at high temperature. *Biochim. Biophys. Acta* 1750, 103–111.
- Grashoff, K., Erhardt, M., Kremling, K., 1983. *Methods in Seawater Analyses*. Verlag Chemie, Weinheim.
- Hastenrath, S., Merle, J., 1987. Annual cycle of subsurface thermal structure in the tropical Atlantic Ocean. *J. Phys. Oceanogr.* 17, 1518–1538.
- Hatta, M., Measures, C.I., Wu, J., Roshan, S., Fitzsimmons, J.N., Sedwick, P., Morton, P., 2014. An overview of dissolved Fe and Mn Distributions during the 2010–2011 U.S. GEOTRACES north Atlantic Cruises: GEOTRACES GA03. *Deep Sea Res. Part II* 116, 117–129.
- Heller, M.I., Gaiero, D.M., Croot, P.L., 2013. Basin scale survey of marine humic fluorescence in the Atlantic: relationship to iron solubility and H<sub>2</sub>O<sub>2</sub>. *Global Biogeochem. Cycles* 27, 88–100.
- Helliwell, K.E., Lawrence, A.D., Holzer, A., Kudahl, U.J., Sasso, S., Krautler, B., Scanlan, D.J., Warren, M.J., Smith, A.G., 2016. Cyanobacteria and eukaryotic algae use different chemical variants of vitamin B<sub>12</sub>. *Curr. Biol.* 26, 999–1008.
- Helmers, E., Schrems, O., 1995. Wet deposition of metals to the tropical North and the South Atlantic Ocean. *Atmos. Environ.* 29, 2475–2484.
- Heywood, J.L., Zubkov, M.V., Tarran, G.A., Fuchs, B.M., Holligan, P.M., 2006. Prokaryoplankton standing stocks in oligotrophic gyre and equatorial provinces of the Atlantic Ocean: evaluation of inter-annual variability. *Deep Sea Res. Part II* 53, 1530–1547.
- Ji, Y., Sherrill, R.M., 2008. Differential effects of phosphorus limitation on cellular metals in *Chlorella* and *Microcystis*. *Limnol. Oceanogr.* 53, 1790–1804.
- Jickells, T.D. et al., 2005. Global iron connections between desert dust, ocean biogeochemistry and climate. *Science* 308, 67–71.
- Johnson, K.S., Gordon, R.M., Coale, K.H., 1997. What controls dissolved iron concentrations in the world ocean? *Mar. Chem.* 57, 137–161.
- Jullion, L., Heywood, K.J., Naveira, A., Garabato, A.C., Stevens, D.P., 2010. Circulation and water mass modification in the Brazil-Malvinas Confluence. *J. Phys. Oceanogr.* 40, 845–864.
- Karstensen, J., Stramma, L., Visbeck, M., 2008. Oxygen minimum zones in the eastern tropical Atlantic and Pacific Oceans. *Prog. Oceanogr.* 77, 331–350.
- Kathuria, S., Martiny, A.C., 2011. Prevalence of a calcium-based alkaline phosphatase associated with the marine cyanobacterium *Prochlorococcus* and other ocean bacteria. *Environ. Microbiol.* 13, 74–83.
- Knauer, G.A., Martin, J.H., Gordon, R.M., 1982. Cobalt in north-east Pacific waters. *Nature* 297, 49–51.
- Kaufman, Y.J., Koren, I., Remer, L.A., Tanré, D., Ginoux, P., Fan, S., 2005. Dust transport and deposition observed from the Terra-Moderate Resolution Imaging Spectroradiometer (MODIS) spacecraft over the Atlantic Ocean. *J. Geophys. Res.* 110. <http://dx.doi.org/10.1029/2003JD004436>.
- Kim, G., Church, T.M., 2002. Wet deposition of trace elements and radon daughter systems in the South and equatorial Atlantic atmosphere. *Global Biogeochem. Cycles* 16. <http://dx.doi.org/10.1029/2001gb001407>.
- Küpper, H. et al., 2008. Iron limitation in the marine cyanobacterium *Trichodesmium* reveals new insights into regulation of photosynthesis and nitrogen fixation. *New Phytol.* 179, 784–798.
- Laes, A. et al., 2007. Sources and transport of dissolved iron and manganese along the continental margin of the Bay of Biscay. *Biogeosciences* 4, 181–194.
- Liu, X., Millero, F.J., 2002. The solubility of iron in seawater. *Mar. Chem.* 77, 43–54.
- Lohan, M.C., Aguilar-Islas, A.M., Franks, R.P., Bruland, K.W., 2005. Determination of iron and copper in seawater at pH 1.7 with a new commercially available chelating resin, NTA Superflow. *Anal. Chim. Acta* 530, 121–129.
- Longhurst, A., 1998. *Ecological Geography of the Sea*. Academic Press, San Diego.
- Mackey, K.R.M., Chien, C.-T., Post, A.F., Saito, M.A., Paytan, A., 2015. Rapid and gradual modes of aerosol trace metal dissolution in seawater. *Front. Microbiol.* 5, 1–11.
- Mahaffey, C., Reynolds, S., Davis, C.E., Lohan, M.C., 2014. Alkaline phosphatase activity in the subtropical ocean: insights from nutrient, dust and trace metal addition experiments. *Front. Mar. Sci.* 1. <http://dx.doi.org/10.3389/fmars.2014.00073>.
- Mahowald, N. et al., 1999. Dust sources and deposition during the last glacial maximum and current climate: a comparison of model results with paleodata from ice cores and marine sediments. *J. Geophys. Res.* 104, 15895–15916.
- Martin, J.H., Gordon, R.M., 1988. Northeast Pacific iron distributions in relation to phytoplankton productivity. *Deep-Sea Res.* 35, 177–196.
- Martin, J.H., 1990. Glacial-interglacial CO<sub>2</sub> change: the iron hypothesis. *Paleoceanography* 5, 1–13.
- Mather, R.L. et al., 2008. Phosphorus cycling in the North and South Atlantic Ocean subtropical gyres. *Nat. Geosci.* 1, 439–443.
- Mawji, E., Gledhill, M., Milton, J.A., Tarran, G.A., Ussher, S., Thompson, A., Wolff, G.A., Worsfold, P.J., Achterberg, E.P., 2008. Hydroxamate Siderophores: occurrence and importance in the Atlantic Ocean. *Environ. Sci. Technol.* 42, 8675–8680.
- Measures, C.I., Landing, W.M., Brown, M.T., Buck, C.S., 2008. High-resolution Al and Fe data from the Atlantic Ocean CLIVAR-CO<sub>2</sub> repeat hydrography A16N transect: extensive linkages between dust and upper ocean geochemistry. *Global Biogeochem. Cycles* 22. <http://dx.doi.org/10.1029/2007GB003042>.
- Mémerly, L. et al., 2000. The water masses along the western boundary of the south and equatorial Atlantic. *Prog. Oceanogr.* 47, 69–98.
- Mills, M.M., Ridame, C., Davey, M., La Roche, J., Geider, R.J., 2004. Iron and phosphorus co-limit nitrogen fixation in the eastern tropical North Atlantic. *Nature* 429, 292–294.
- Moffett, J.W., Ho, J., 1996. Oxidation of cobalt and manganese in seawater via a common microbially catalyzed pathway. *Geochim. Cosmochim. Acta* 60, 3415–3424.
- Moore, M.C. et al., 2009. Large-scale distribution of Atlantic nitrogen fixation controlled by iron availability. *Nat. Geosci.* 2, 867–871.
- Moore, C.M. et al., 2013. Processes and patterns of oceanic nutrient limitation. *Nat. Geosci.* 6, 701–710.
- Moore, C.M., Mills, M.M., Milne, A., Langlois, R., Achterberg, E.P., Lochte, K., Geider, R.J., La Roche, J., 2006. Iron limits primary productivity during spring bloom development in the central North Atlantic. *Glob. Change Biol.* 12, 626–634.
- Moore, J.K., Doney, S.C., Glover, D.M., Fung, I.Y., 2002. Iron cycling and nutrient-limitation patterns in surface waters of the World Ocean. *Deep Sea Res. Part II* 49, 463–507.
- Morel, F.M.M., Reinfelder, J.R., Roberts, S.B., Chamberlain, C.P., Lee, J.G., Yee, D., 1994. Zinc and carbon co-limitation of marine phytoplankton. *Nature* 369, 740–742.
- Morel, F.M.M., Price, N.M., 2003. The biogeochemical cycles of trace metals in the oceans. *Science* 300, 944–947.
- Nielsdottir, M.C., Moore, C.M., Sanders, R., Hinz, D.J., Achterberg, E.P., 2009. Iron limitation of the post bloom phytoplankton communities in the Iceland Basin. *Global Biogeochem. Cycles* 23. <http://dx.doi.org/10.1029/2008GB003410>.
- Noble, A.E., Saito, M.A., Maiti, K., Benitez-Nelson, C., 2008. Cobalt, manganese, and iron near the Hawaiian Islands: a potential concentrating mechanism for cobalt within a cyclonic eddy and implications for the hybrid-type trace metals. *Deep Sea Res. Part II* 55, 1473–1490.
- Noble, A.E. et al., 2012. Basin-scale inputs of cobalt, iron, and manganese from the Benguela-Angola front to the South Atlantic Ocean. *Limnol. Oceanogr.* 57, 989–1010.
- Obata, H., Karatani, H., Nakayama, E., 1993. Automated determination of iron in seawater by chelating resin concentration and chemiluminescence detection. *Anal. Chem.* 65, 1524–1528.
- Pohl, C., Croot, P.L., Hennings, U., Daberkow, T., Budeus, G., Rutgers van der Loeff, M., 2010. Synoptic transects on the distribution of trace elements (Hg, Pb, Cd, Cu, Ni, Zn, Co, Mn, Fe, and Al) in surface waters of the Northern and Southern East Atlantic. *J. Mar. Syst.* 84, 24–41.
- Powell, C.F., Baker, A.R., Jickells, T.D., Bange, H.W., Chance, R.J., Yodanis, C., 2015. Estimation of the atmospheric flux of nutrients and trace metals to the eastern tropical North Atlantic Ocean. *J. Atmos. Sci.* 4029–4045.
- Prospero, J.M., Carlson, T.N., 1972. Vertical and areal distribution of Saharan dust over the Equatorial North Atlantic Ocean. *J. Geophys. Res.* 77, 5255–5265.
- Prospero, J.M., Ginoux, P., Torres, O., Nicholson, S.E., Thomas, T.E., 2002. Environmental characterization of global sources of atmospheric dust identified with the Nimbus 7 Total Ozone Mapping Spectrometer (TOMS) absorbing aerosol product. *Rev. Geophys.* 40. <http://dx.doi.org/10.1029/2000RG000095>.
- Richier, S., Macey, A.I., Pratt, N.J., Honey, D.J., Moore, C.M., Bibby, T.S., 2012. Abundances of iron-binding photosynthetic and nitrogen-fixing proteins of *Trichodesmium* both in culture and in situ from the North Atlantic. *PLoS One* 7. <http://dx.doi.org/10.1371/journal.pone.0035571>.
- Ridame, C., Moutin, T., Guieu, C., 2003. Does phosphate adsorption onto Saharan dust explain the unusual N/P ratio in the Mediterranean Sea? *Oceanol. Acta* 26, 629–634.
- Rijkenberg, M.J.A., Middag, R., Laan, P., Gerringa, L.J.A., van Aken, H.M., Schoemann, V., de Jong, J.T.M., de Baar, H.J.W., 2014. The distribution of dissolved iron in the West Atlantic Ocean. *PLoS One* 9. <http://dx.doi.org/10.1371/journal.pone.0101323>.
- Rijkenberg, M.J.A., Steigenberger, S., Powell, C.F., van Haren, H., Patey, M.D., Baker, A.R., Achterberg, E.P., 2012. Fluxes and distribution of dissolved iron in the eastern (sub-) tropical North Atlantic Ocean. *Global Biogeochem. Cycles* 26. <http://dx.doi.org/10.1029/2011gb004264>.
- Robinson, C., 2006. The Atlantic Meridional Transect (AMT) programme: a contextual view 1995–2005. *Deep Sea Res. Part II: Top. Stud. Oceanogr.* 53, 1485–1515.
- Rodriguez, I.B., Ho, T.-Y., 2015. Influence of Co and B<sub>12</sub> on the growth and nitrogen fixation of *Trichodesmium*. *Front. Microbiol.* 6. <http://dx.doi.org/10.3389/fmicb.2015.00623>.
- Roshan, S., Wu, J., 2015. Water mass mixing: the dominant control on the zinc distribution in the North Atlantic Ocean. *Global Biogeochem. Cycles* 29, 1060–1074.
- Rubin, M., Berman-Frank, I., Shaked, Y., 2011. Dust-and mineral-iron utilization by the marine dinitrogen-fixer *Trichodesmium*. *Nat. Geosci.* 4, 529–534.
- Rudnick, R.L., Gao, S., 2003. Composition of the continental crust. In: Holland, H.D., Turckian, K.K. (Eds.), *Treatise on Geochemistry*. Elsevier, Oxford, pp. 1–64.
- Saito, M.A., Goepfert, T.J., 2008. Zinc-cobalt colimitation of *Phaeocystis antarctica*. *Limnol. Oceanogr.* 53, 266–275.
- Saito, M.A., Goepfert, T.J., Ritt, J.T., 2008. Some thoughts on the concept of colimitation: three definitions and the importance of bioavailability. *Limnol. Oceanogr.* 53, 276–290.
- Saito, M.A., Moffett, J.W., 2001. Complexation of cobalt by natural organic ligands in the Sargasso Sea as determined by a new high-sensitivity electrochemical cobalt speciation method suitable for open ocean work. *Mar. Chem.* 75, 49–68.
- Saito, M.A., Moffett, J.W., 2002. Temporal and spatial variability of cobalt in the Atlantic Ocean. *Geochim. Cosmochim. Acta* 66, 1943–1953.
- Saito, M.A., Moffett, J.W., Chisholm, S., Waterbury, J.B., 2002. Cobalt limitation and uptake in *Prochlorococcus*. *Limnol. Oceanogr.* 47, 1629–1636.

- Saito, M.A., Rocap, G., Moffett, J.W., 2005. Production of cobalt binding ligands in a *Synechococcus* feature at the Costa Rica upwelling dome. *Limnol. Oceanogr.* 50, 279–290.
- Sanudo-Wilhelmy, S.A., Kustka, A.B., Gobler, C.J., Hutchins, D.A., Yang, M., Lwiza, K., Burns, J., Capone, D.G., Raven, J.A., Carpenter, E.J., 2001. Phosphorus limitation of nitrogen fixation by *Trichodesmium* in the central Atlantic Ocean. *Nature* 411, 66–69.
- Sarthou, G. et al., 2003. Atmospheric iron deposition and sea-surface dissolved iron concentrations in the eastern Atlantic Ocean. *Deep Sea Res. Part I: Oceanogr. Res. Pap.* 50, 1339–1352.
- Sarthou, G. et al., 2007. Influence of atmospheric inputs on the iron distribution in the subtropical North-East Atlantic Ocean. *Mar. Chem.* 104, 186–202.
- Schattenhofer, M., Fuchs, B.M., Amann, R., Zubkov, M.V., Tarran, G.A., Pernthaler, J., 2009. Latitudinal distribution of prokaryotic picoplankton populations in the Atlantic Ocean. *Env. Microbiol.* 11. <http://dx.doi.org/10.1111/j.1462-2920.2009.01929.x>.
- Schattenhofer, M., Wulf, J., Kostadinov, I., Glöckner, F.O., Zubkov, M.V., Fuchs, B.M., 2011. Phylogenetic characterisation of picoplanktonic populations with high and low nucleic acid content in the North Atlantic Ocean. *System. Appl. Microbiol.* 34, 470–475.
- Schlosser, C. et al., 2013. Seasonal ITCZ migration dynamically controls the location of the (sub)tropical Atlantic biogeochemical divide. *Proc. Natl. Acad. Sci.* <http://dx.doi.org/10.1073/pnas.1318670111>.
- Shaked, Y., Lis, H., 2012. Dissassembling iron availability to phytoplankton. *Front. Microbiol.* 3. <http://dx.doi.org/10.3389/fmicb.2012.00123>.
- Shelley, R.U., Morton, P.L., Landing, W.M., 2015. Elemental ratios and enrichment factors in aerosols from the US-GEOTRACES North Atlantic transects. *Deep Sea Res. Part II: Top. Stud. Oceanogr.* 116, 262–272.
- Shelley, R.U. et al., 2012. Controls on dissolved cobalt in surface waters of the Sargasso Sea: Comparisons with iron and aluminum. *Global Biogeochem. Cycles* 26. <http://dx.doi.org/10.1029/2011gb004155>.
- Shelley, R.U., Zachhuber, B., Sedwick, P.J., Worsfold, P.J., Lohan, M.C., 2010. Determination of total dissolved cobalt in UV-irradiated seawater using flow injection with chemiluminescence detection. *Limnol. Oceanogr: Meth.* 8, 352–362.
- Sholkovitz, E.R., Copland, D., 1981. The coagulation, solubility and adsorption properties of Fe, Mn, Cu, Ni, Cd, Co and humic acids in a river water. *Geochim. Cosmochim. Acta* 45, 181–189.
- Sultan, B., Janicot, S., 2000. Abrupt shift of the ITCZ over West Africa and intra-seasonal variability. *Geophys. Res. Lett.* 27, 3353–3356.
- Sunda, W.G., Huntsman, S.A., 1995a. Cobalt and zinc inter-replacement in marine phytoplankton: biological and geochemical implications. *Limnol. Oceanogr.* 40, 1404–1417.
- Sunda, W.G., Huntsman, S.A., 1995b. Iron uptake and growth limitation in oceanic and coastal phytoplankton. *Mar. Chem.* 50, 189–206.
- Tarran, G.A., Heywood, J.L., Zubkov, M.V., 2006. Latitudinal changes in the standing stocks of nano- and picoeukaryotic phytoplankton in the Atlantic Ocean. *Deep Sea Res. Part II* 53, 1516–1529.
- Thuroczy, C.-E., Boye, M., Losno, R., 2010. Dissolution of cobalt and zinc from natural and anthropogenic dusts in seawater. *Biogeosciences* 7, 1927–1936.
- Timmermans, K.R., Snoek, J., Gerringa, L.J.A., Zondervan, I., de Baar, H.J.W., 2001. Not all eukaryotic algae can replace zinc with cobalt: *Chaetoceros calcitrans* (Bacillariophyceae) versus *Emiliania huxleyi* (Prymnesiophyceae). *Limnol. Oceanogr.* 46, 699–703.
- Tsamalis, C., Chédin, A., Pelon, J., Capelle, V., 2013. The seasonal vertical distribution of the Saharan Air Layer and its modulation by the wind. *Atmos. Chem. Phys.* 13, 11235–11257.
- Tyrrell, T., Maranon, E., Poulton, A.J., Bowie, A.R., Harbour, D.S., Woodward, E.M.S., 2003. Large-scale latitudinal distribution of *Trichodesmium* spp. in the Atlantic Ocean. *J. Plankton Res.* 25, 405–416.
- Ussher, S.J. et al., 2013. Impact of atmospheric deposition on the contrasting iron biogeochemistry of the North and South Atlantic Ocean. *Global Biogeochem. Cycles* 27, 1096–1107. <http://dx.doi.org/10.1002/gbc.20056>.
- Ussher, S.J. et al., 2007. Distribution and redox speciation of dissolved iron on the European continental margin. *Limnol. Oceanogr.* 52, 2530–2539.
- Vega, M., van den Berg, C.M.G., 1997. Determination of cobalt in seawater by catalytic adsorptive cathodic stripping voltammetry. *Anal. Chem.* 69, 874–881.
- Welschmeyer, N.A., 1994. Fluorometric Analysis of chlorophyll a in the presence of chlorophyll b and pheopigments. *Limnol. Oceanogr.* 39, 1985–1992.
- Westrich, J.R., Ebling, A.M., Landing, W.M., Joyner, J.L., Kemp, K.M., Griffin, D.W., Lipp, E.K., 2016. Saharan dust nutrients promote *Vibrio* bloom formation in marine surface waters. *Proc. Natl. Acad. Sci.* 113, 5964–5969.
- Wong, G.T.F., Pai, S.-C., Chung, S.-W., 1995. Cobalt in the West Philippine Sea. *Oceanol. Acta* 18, 631–638.
- Woodward, E.M.S., Rees, A.P., Stephens, J.A., 1999. The influence of the south-west monsoon upon the nutrient biogeochemistry of the Arabian Sea. *Deep Sea Res.: Part II* 46, 571–591.
- Wu, J., Boyle, E., Sunda, W., Wen, L.-S., 2001. Soluble and colloidal iron in the oligotrophic North Atlantic and North Pacific. *Science* 293, 847–849.
- Wu, J., Roshan, S., Chen, G., 2014. The distribution of dissolved manganese in the tropical–subtropical North Atlantic during US GEOTRACES 2010 and 2011 cruises. *Mar. Chem.* 166, 9–24.
- Wyatt, N.J. et al., 2014. Biogeochemical cycling of dissolved zinc along the GEOTRACES South Atlantic transect GA10 at 40°S. *Global Biogeochem. Cycles* 28, 44–56.